Sedimentary characteristics of hybrid event beds in deep-lacustrine basins and their impact on reservoir quality: examples from the Bohai Bay Basin, Eastern China

Zehua Zhang[a,b,c,d], Hongliang Wang[a,b,c*], Thomas J. H. Dodd[e], and Shige Shi

[a] School of Energy Resources, China University of Geosciences (Beijing), Beijing 100083, China

[b] Key Laboratory of Marine Reservoir Evolution and Hydrocarbon Enrichment Mechanism, Ministry of Education, China University of Geosciences (Beijing), Beijing 100083, China

[c] Beijing Key Laboratory of Unconventional Natural Gas Geological Evaluation and Development Engineering, China University of Geosciences (Beijing), Beijing 100083, China

[d] China United Coalbed Methane Corp., Ltd, Beijing 100011, China

[e] British Geological Survey, the Lyell Centre, Research Avenue South, Edinburgh, EH144AP, UK

[f] Shengli Oilfield Company, SINOPEC, Dongying 257000, China

* Correspondence: Whliang@cugb.edu.cn; Tel.: +86-010-82321865

Abstract

Hybrid event beds (HEBs) form important components of subaqueous sediment gravity flow models in deep-lacustrine sedimentary basins, largely due to their clay-rich nature meaning that they often form non-reservoir and/or baffles/barriers to fluid flow in the subsurface. Using examples from a typical deep-lacustrine basin, this study documents the sedimentary characteristics and distribution of HEBs and explores their effect on reservoir properties. To achieve this, a suite of drill cores and wireline data through a range of debrites, concentrated flow deposits, and turbidites are analyzed from Paleogene in the Bohai Bay Basin, China. The superposition and convergence of gravity flow deposits resulted in a complex spatial and temporal distribution and evolution of the HEBs in the study area. The majority of identified HEB types are interpreted to be associated with lobe deposition. However, slumping-induced HEBs are interpreted to be restricted to the proximal slump areas. Slump HEBs are interpreted to have formed through slumping and associated generation of sediment gravity flows, where HEBs formed through flow transformation of slumps into high-

concentration flows (debris flows) and/or high-density turbidity currents in down-slope areas. Debris flow HEBs are interpreted to be formed by particle rearrangement through vertical settling during flow transformation within the subaqueous fans. The effects of relative buoyancy in debris flows, rearrangement of debris flow particles, muddy substrate erosion by turbidity currents, and slumping upon HEB development is discussed. The average porosity and permeability observed within reservoir intervals formed by gravity flow deposits is 17.8% (ranging from 2% to 25%) and 126 mD (ranging from 3mD to 816 mD), respectively. HEBs within the studied reservoir interval display low-porosity (<15% on average) and low-permeability (<10 mD on average) values. The occurrence of HEBs within a reservoir increases the variation coefficient of permeability, quantity, and thickness of the interlayers and presents a significant heterogeneity. The results of this study are important to consider in the context of constructing reservoir models in deep-lacustrine reservoirs of the Bohai Bay Basin, and which can be applied to other lacustrine gravity flow deposits in sedimentary basins worldwide.

Keywords: Hybrid event beds (HEBs); gravity flow deposits; sedimentary characteristics; reservoir properties; Bohai Bay Basin

1. Introduction

With the researches on gravity flow deposits deepening, the flow transformation and their complex products in the sediment gravity flow spectrum with two end-members (debris flows and turbidity currents) have been focused (e.g. Lowe, 1982; Mulder and Alexander, 2001; Talling *et al*., 2012; Tan *et al*., 2016). In the sediment gravity flow spectrum, hybrid event beds (HEBs) generally comprising a basal sandstone division and overlying mud-rich division have been documented in studies (e.g. Lowe, 1976; Lowe and Guy, 2000; Haughton *et al.,* 2003; Jackson *et al.,* 2009; Felix and Peakall, 2010; Lowe *et al.,* 2010; Girard *et al*., 2012; Grundvag *et al.,* 2014; Mueller *et al*., 2017; Baas *et al*., 2021). Haughton et al. (2009) summarized an idealized sequence of HEBs, which contains five divisions including (from bottom to top): clean sandstone (H1), banded sandstone (H2), chaotic muddy sandstone (H3), stratified sandstone (H4), and mudstone (H5). Furthermore, according to the internal variation, H1 division has been sub-divided into H1a and H1b, and H3 division has been sub-divided into H3a, H3b and H3c (Fonnesu *et al.,* 2015; Pierce *et al*., 2018; Hussain *et al.*, 2020; Shan *et al*., 2021; Dodd *et al.*, 2022). HEBs can be observed in the proximal environment, distal environment and channel-lobe transition zone of gravity flow depositional system (e.g. Haughton *et al*., 2009; Hodgson, 2009; Talling *et al*., 2012; Fonnesu *et al.,* 2015; Pierce *et al.,* 2018; Yang *et al.,* 2018). In fact, a single event bed does not necessarily contain all the divisions mentioned above and HEBs' distribution is scattered, which increases the variability of HEBs' characteristic and distribution. As opposed to deposits caused by a single flow (e.g. cohesive flow or turbidity current), HEBs exhibiting 'mixed' behavior are often caused by a variety of flows, for instance, the H1 and H3 are respectively regarded as the product of turbulence and cohesive debris flows (Haughton *et al*., 2009; Fonnesu *et al*., 2016; Patacci *et al*., 2020). The formation of HEBs usually comes along with flow transformation, the dampening of turbulence and both vertical and longitudinal particle rearrangement or segregation (Haughton *et al.,* 2003; Talling *et al.,* 2004;

Talling *et al.,* 2007; Felix *et al.,* 2009; Haughton *et al.,* 2009; Felix and Peakall, 2010; Talling, 2013; Baker and Baas, 2020; Jin *et al*., 2021; Mansor and Amir Hassan, 2021). Up to now, some origins such as 'the deceleration of flows' and 'the erosion of turbulence' have been proposed to explain the formation of HEBs, although the origin of HEBs is still debated (Cao *et al*., 2017). In general, given the complex origin, distribution and characteristic of HEBs, additional investigations about HEBs are still required, which is especially true for HEBs in lacustrine basins with less documents.

In addition, lacustrine gravity flows can form extensive coarse-grained and associated fine-grained clastic deposits in deep lakes, which fundamentally control the loci and volume of hydrocarbon accumulation, and reservoir heterogeneity. As a consequence of their clay-rich matrices, HEBs are well-known to form lower-quality and lower pore-volume reservoirs, and can act as vertical fluid transmissibility barriers in deepwater fan hydrocarbon reservoirs (Haughton *et al.*, 2003; Amy *et al.*, 2006, 2009; Davis *et al*, 2009; Kane and Pontén, 2012; Fonnesu *et al.*, 2015). It is therefore important to investigate where these deposits occur spatially across and throughout a deep-lacustrine fan system, and how this may relate to the variability in HEB internal character during fan evolution. This has implications on reservoir modelling, both in terms of predictability and in their potential effect on hydrocarbon production (e.g., the use of enhanced production methodologies; Fonnesu *et al.*, 2015). Distinct deep-lacustrine gravity flow deposits are widely distributed in the lower group of the third member of Shahejie Formation in the Eocene (Es_{3L}) in the Gubei Sag (Bohai Bay Basin, China) (Fig. 1), which makes this location ideal for studying the origin and sedimentary characteristics of HEBs and their influence upon reservoir heterogeneity (Teng, 2016; Zhang and Wang, 2023).

In this study, core, well log, and reservoir property data of deep-lacustrine gravity flow deposits in the Es_{3L} from the Gubei sag are analyzed to (a) identify the HEB types and their sedimentary characteristics, (b)

define the spatial and temporal distributions of HEBs, (c) evaluate the evolution of lacustrine gravity flow deposits with HEBs of different origins, and (d) consider the relationship between HEBs and reservoir heterogeneity. Through this analysis, the new research on HEBs provides important insights into their controlling influence upon hydrocarbon reservoir properties; the generic value of these insights can be applied to analogous deep-lacustrine fan reservoirs in other basins worldwide.

2. Geological setting

The Gubei Sag is located in the east of the Jiyang Depression in the Bohai Bay Basin (Fig. 1a). It is bounded by the Zhuangnan, Changdi, Gubei, and Chengdong faults and contains two sub-sags in the north, one uplift structure in the east, three steep fault zones in the west, and a gentle fault zone in the south (Fig. 1b) (Shi and Zhao, 2003, Zhuang *et al.*, 2003; Zhao, 2007; Teng, 2016).

The Gubei Sag forms as a rift basin related to Cenozoic tectonism and subsequent sedimentary infill (Fig. 1c). The sedimentary succession in the Gubei Sag primarily contains Paleogene and Neogene strata (Fig. 1c). The Paleogene and Neogene strata have been sub-divided, with the Eocene to Oligocene part of the succession being divided into the Kongdian, Shahejie, and Dongying formations, whilst the Neogene interval being divided into the Guantao and Minghuazhen formations (Fig. 1c). Among them, the third member of Eocene Shahejie Formation (Es_3) composed of dark grey oil shales, dark grey mudstones, sandstones, siltstones, and pebbly sandstones is the primary hydrocarbon-bearing interval in the Gubei sag, which is further sub-divided informally into the lower unit (Es_{3L}), middle unit (Es_{3M}) and upper unit (Es_{3U}) from bottom to top (Fig. 1c) (Zhang *et al.*, 2002;Liao, 2021; Teng, 2016). During the Es_{3L} times, increased paleo-water depth, intense rifting tectonic activity and warm and humid climates increased the accommodation and the frequency of flood, and enhanced hydrodynamic force (Fig. 1c) (Li et al., 2017), causing the detritus

sourced from Changdi salient enter the paleo-lake to form five deep-lacustrine flood-generated fans (Fig. 1d) (Zhang and Wang, 2023). Each deep-lacustrine fan consists of levee, channel, as well as lobe elements. The five deep-lacustrine fans originate mainly from the southern and eastern part of the Gubei Sag, and are all vertically connected with each other, forming a stacked succession (Zhang and Wang, 2023). In-addition to the main fans, relatively small (approximately 10 km^2) oval-shaped slumps are observed in front of the deep-lacustrine fans, which are spatially associated with observed faults (Fig. 1d) (Zhang and Wang, 2023). Understanding the HEBs' sedimentary characteristics in the deep-lacustrine fans and slumps within Es_{3L} as well as HEBs' influences on reservoirs forms the main objective of this study.

3. Methodology

Three data sets from Gubei sag in Es_{3L} times are used in this study, including data from 712 meters of drill core, wireline data from 317 wells, and 126 permeability and porosity sample points measured by the 'perm-plug' method (Muskat, 1937). The cores are used to identify the lithofacies and sedimentary characteristics of HEBs. Wireline data are used to identify the sedimentary facies along the non-cored intervals. The flow types, distribution, and origin of the HEBs were identified based on internal boundaries, sedimentary facies, and lithofacies analysis. The average permeability of the interval of interest is leveraged to analyze the heterogeneity of the reservoir. Using these three datasets, the control of HEBs upon reservoir heterogeneity was investigated and evaluated.

Four terms are frequently used in this paper: turbidity current, concentrated flow, debris flow, and cohesive flow. Different flow types exhibit specific grain-support mechanisms and flow rheologies that deposit particular sedimentary features (Fig. 2). The term turbidity current denotes low-density turbulent flow (Middleton and Hampton, 1973; Mulder and Alexander, 2001), of which the deposits present complete Bouma sequence or the upper part of Bouma sequence (Tc-e divisions) (Bouma, 1962). The term concentrated flow

is applied in the same sense as 'high-density turbulent flow' (*sensu* Lowe, 1982; Shanmugam, 2000; Mulder and Alexander, 2001; Shanmugam, 2013; Pickering and Hiscott, 2015), in which the grains are supported by hindered settling and grain interaction. The concentrated flow deposits usually are composed of graded and stratified sandstones and overlying mudstones, and occasionally present the lower part of Bouma sequence (Ta-b divisions) (Bouma, 1962; Lowe, 1982; Pickering and Hiscott, 2015). Debris flows can be divided based on differences in the matrix cohesive mud content into cohesive flows (generally *ca* > 12%) and sandy debris flows (generally *ca* < 12%; Talling *et al.*, 2012). Cohesive flows have a high bulk concentration in which the particles are mainly transported by frictional forces and the final deposition from these flows occurs by cohesive freezing '*en masse*' (Pickering *et al.,* 1986; Pickering and Hiscott, 2015). In comparison, grain collisions and pore pressure are the primary particle-support mechanisms of sandy debris flow (Postma, 1986; Pickering and Hiscott, 2015). In the Results, Discussion and Conclusion chapters of this paper, the term sandy debris flow is replaced by debris flow. The terms 'tripartite' and 'bipartite' are used to denote the vertical stacking structures of the event beds.

4. Results

4.1 Lithofacies

Observation on drill cores revealed the presence of a range of lithologies, including: pebbly sandstone, sandstone, muddy sandstone, muddy siltstone, siltstone, and mudstone (Fig. 3). These lithologies were divided into 13 separate lithofacies, based on contained sedimentary structures and interpreted sedimentary processes of emplacement (Table 1). These facies have been described in detail, interpreted for sedimentary processes of emplacement, and form the key lithofacies building blocks for the sedimentary model developed in this study.

4.2 Lithofacies associations

Ten lithofacies associations (LA) have been recognized, described, and interpreted based on the observed lithofacies and their vertically stacking patterns (Figs 4–7). LA 1, LA 2, LA 3 and LA 5 correspond to non-cohesive flow deposits, LA 4 corresponds to sediment failure, whereas LA 6–9 represent a wide range of bed types that correspond to HEB deposition (*sensu* Haughton *et al.*, 2009).

4.2.1 LA 1: Structureless pebbly sandstone and mudstone

Description: LA 1 consists predominantly of structureless pebbly sandstones (*fmps*) and overlying structureless mudstones (*fmm*) (Fig. 4a). Dispersed phytodetritus and mud-clasts are observed in structureless pebbly sandstones (Fig. 4a). LA 1 ranges from 0.35 m to 1 m in thickness, and the boundary between the structureless pebbly sandstone (*fmps*) and overlying structureless mudstones (*fmm)* usually is sharp (Fig. 4a). Erosional base can be observed occasionally. Graded pebbly sandstones (*fgps*) or stratified pebbly sandstones (*fsps*) underlie these beds.

Interpretation: Dark grey structureless mudstones (*fmm*) within this LA are interpreted as the deposition of suspended mud (Yang, et al., 2019). Dispersed mud-clasts indicate that structureless pebbly sandstones were deposited through *en masse* freezing of a debris flow (Lowe, 1982; Talling et al., 2012). The erosional base and graded pebbly sandstones (*fgps*) underlying LA 1 imply that the debris flow generating the structureless pebbly sandstones is formed by the transformation of turbulence. A few mud clasts mix into flows through flow erosion, causing the damping of turbulence then forming structureless pebbly sandstones. Warm and humid climate during Es_{3L} times (Li, et al., 2017), coupled with the existence of phytodetritus, jointly indicate that lacustrine gravity flow deposits may have been generated by flooding from the hinterland or slope collapse caused by flooding (*sensu* Zavala and Pan, 2018; Zhang and Wang, 2023).

4.2.2 LA 2: Graded and stratified pebbly sandstone and mudstone

Description: LA 2 comprise inverse-then-normal graded (*fgps*) or stratified pebbly sandstones (*fgps* and/or *fsps*) that contain phytodetritus (Fig. 4b) and occasional mudstones (*fmm*) which are observed to overlie or underlie the pebbly sandstones (*fgps*/*fsps*), with erosional base and sharp upper contact. The thickness of individual beds ranges from 0.3 m to 1.2 m. Normally graded pebbly sandstones are thicker than inversely graded or stratified pebbly sandstones. Erosion surfaces are sometimes observed near the base of normally graded pebbly sandstones (Fig. 4b). There are no clear boundaries between the normally and inversely graded pebbly sandstones.

Interpretation: The horizontal arrangement of gravels in stratified pebbly sandstones (*fsps*), inverse-then-normal grading in graded pebbly sandstones (*fgps*), and phytodetritus suggest that LA 2 are associated with deposition of the bedload of hyperpycnal flows (Zavala and Arcuri, 2016; Zavala, 2020). Alternatively, stratified pebbly sandstones (*fsps*) or graded pebbly sandstones (*fgps*) can be formed by suspension fallout or collapse of near-bed traction carpets beneath concentrated flows (Sohn, 1997; Pickering and Hiscott, 2015). Hyperpycnal flows are regarded as a special type of concentrated flow according to its similarity with concentrated flows (Yang *et al.*, 2019). Thus, LA 2 with amalgamated pebbly sandstones are considered to be formed by concentrated flows and interpreted as channel-fill elements based on the erosion.

4.2.3 LA 3: Structureless sandstones and mudstones

Description: LA 3 are mainly composed of fine-grained, well sorted structureless sandstones (*fms*) and structureless mudstones (*fmm*), which range from 0.2 m to 1.5 m in thickness. The contact between structureless sandstones (*fms)* and structureless mudstones (*fmm)* is sharp (Fig. 5a). Weak erosional structures are observed at the bottom of structureless sandstones (*fms)*. Floating mud-clasts are observed within the beds, as are discrete layers of mud-clasts at the top of structureless sandstones *(fms)*.

Interpretation: Structureless sandstones and overlying structureless mudstones suggest that LA 3 can be

formed by debris flows or concentrated flows. However, the floating mud-clasts and mud-clast layers at the top of structureless sandstones indicate that LA 3 was formed by the layer-by-layer deposition of concentrated flows (high-density turbidites) rather than the *en masse* deposition of cohesionless debris flows (Talling et al., 2012; Liu *et al.,* 2017; Xian *et al.,* 2018). Structureless mudstones in LA3 is interpreted to be formed by the suspension fallout of mud in deep lake. The fine-grained well-sorted nature of these sediments may indicate that the particles experienced long-distance transportation and/or efficient sorting processes.

4.2.4 LA 4: Deformed sandstones and mudstones

Description: LA 4 only forms in the slump system (Fig. 1, Fig. 5). Convolute structures are commonly observed in LA 4, which have a thickness ranging from 0.1 m to 3 m (Fig. 5b). Large dark grey mud-clasts and layers of mud-clasts are observed in LA 4. The most notable features of LA 4 are the mixed deposition of sand and mud, and soft-sediment fold structures composed of sandstone and mudstone laminae. Pure black mudstones with convolute structures are observed in LA 4.

Interpretation: The formation of convolute structures is induced by a plastically-deforming flow comprising poorly unconsolidated sediments. LA 4 associating with the slump in Gubei sag and the formation of convolute structures jointly indicate that LA 4 is the product of slumping (*sensu* Liu *et al*., 2016; Symons *et al.,* 2016; Southern *et al.,* 2017; Zhang and Wang et al., 2023).

4.2.5 LA 5: Graded and stratified sandstone

Description: Fine-grained typically normally graded sandstones (*fgs*) and parallel-stratified sandstone (*fps*) (Fig. 5c). These beds range from 0.1 m to 0.5 m in thickness. Internal boundaries are observed within LA 5, which form as sharp or gradual contacts. Erosion structures are present at the bottom of the normally graded sandstones (Fig. 5c), below which graded pebbly sandstones (*fgps*) are always present. LA 5 usually is

covered by cross-laminated sandstones/siltstones (*frxbs*).

Interpretation: LA 5 displays parts of the vertical repeated stacking pattern of the Ta-b Bouma sequence. Normally graded sandstones (*fgs*) and parallel-stratified sandstones (*fps*) are linked to Ta and Tb division, respectively. Therefore, LA 5 are considered as being deposited by concentrated flow (high-density turbidity currents) (Bouma, 1962; Talling *et al*., 2012).

4.2.6 LA 6: Ripple cross-bedded sandstones/siltstones and mudstones

Description: LA 6 mainly comprises ripple cross-laminated sandstones or siltstones (*frxbs*), parallel laminated siltstone (*fpss*) and structureless mudstones (*fmm*) (Fig. 5c). These beds range from 0.1 m to 0.5 m in thickness. There are no clear boundaries observed within LA 6 (Fig. 5c). Occasionally, the repeated stacking of ripple cross-laminated sandstones/siltstone (*frxbs*) and underlying parallel-stratified sandstone (*fps*) is observed.

Interpretation: LA 6 shows the vertical repeated stacking pattern of the Bouma Tc-e divisions. Ripple cross-laminated sandstones or siltstone (*frxbs*), parallel laminated siltstone (*fpss*) and structureless mudstones (*fmm*) are linked to Tc, Td, and Te division, respectively. Consequently, LA 6 is considered as being deposited by turbidity currents (low-density turbidity currents) (Bouma, 1962). The repeated stacking of Tc Bouma unit and underlying parallel-stratified sandstone (*fps*) may have arisen from dynamic changes of turbidity currents (Ge *et al.,* 2022).

4.2.7 LA 7: Fine-grained sandstone and muddy siltstone

Description: LA 7 ranges from 0.2 m to 0.85 m in thickness and comprises fine-grained sandstones (*fgs*) and muddy siltstones (*fcmss*). LA 7 are divided into two divisions according to the internal lithofacies (Fig. 6a). The lower division is composed of fine-grained sandstones (*fgs*) that display faint normal grading and water

escape structures at the top. The lower division has a sharp contact with the underlying structureless mudstones (*fmm*) and overlying muddy siltstones (*fcmss*). The upper division consists of black or grey mud clast-poor muddy siltstones (*fcmss*) that lack an erosional basal contact. Mud-clasts in muddy siltstones (*fcmss*) are comparatively smaller than those in other lithofacies associations. Muddy siltstones (*fcmss*) have an average thickness of 0.26 cm, which is slightly thicker than that of the fine-grained sandstones (*fgs*) in the lower division (the average thickness is 0.22 cm). Sandstones above the upper division range from 0.05 m to 0.25 m in thickness and consist of structureless sandstones (*fms*) in the lower part and parallel-stratified sandstones (*fps*) in the upper part. The boundaries are sharp between the sandstones and upper division of these bed types.

Interpretation: LA 7 are interpreted to have formed by the settling down of particles in a preceding or underlying relatively low-density flow and the *en masse* freezing of an ensuing or overlying cohesive flow caused by the buoyancy of low-density debris (clasts) (Fig. 8a). The formation process of LA 7 is similar to that of the 'HEB3' bed-types described by Pierce et al. (2018). The presence of weakly-normally graded sandstones (*fgs*) indicates that the formation of the lower division was induced by the suspension fallout of concentrated flows or aggradation of decelerating turbidity currents (Pickering and Hiscott, 2015; Yang *et al.,* 2022). Dispersed mud-clasts in the upper division are smaller and better sorted compared with that in the divisions representing 'H3' division of HEBs within other lithofacies associations, suggesting that they have been efficiently transported (long distance transportation), and may have provided a source for additional dispersed clays within flows through down-flow attritional process. The absence of erosional base indicates that the transformation from turbulence to cohesive flow generating the upper division is not caused by erosion. The water escape structures demonstrate that particles moved upward under the influence of pore pressure and buoyancy during deposition. Through the action of buoyancy and pore pressure, low-density

debris (clasts) moved vertically-upward in the flow, leading to an increase in the mud-clast content in the upper part of the turbidity current. In addition to this, upwards and rearward (longitudinal) segregation of mud-grade material within the flow structure occurred, which leads to the dampening of turbulence and transformation to cohesive flow types (Fig. 8a) (Talling *et al.,* 2004; Pritchard and Gladstone, 2009).

LA 7 commonly lacks mudstone caps (the 'H5' part of HEBs) and overlying stratified sandstones (*fps*), suggesting the erosion of the bed tops by subsequent flows, and therefore overall aggradation or progradation of the fan systems into the basin center. As the sandstones in the lower division have the same mean grain size as that observed in the beds directly above LA 7, they are interpreted to be genetically un-related deposits and should be considered as products of separate event beds (*sensu* Mutti *et al.*, 2003).

4.2.7 LA 8: Clean sandstone and clast-rich muddy sandstone

Description: LA 8 consists of weakly-normally graded sandstones (*fgs*) in the lower division and clast-rich muddy sandstones (*fcms*) in the upper division (Fig. 6b). The boundaries are typically sharp between the lower and upper divisions. Large chaotically distributed mud-clasts and convolute structures are observed in the upper division (Fig. 6b). The upper division contains more thickly-bedded muddy sandstones (*fcms*) (average thickness of 0.92 m) than compared with all other lithofacies associations. And the upper division are three times thicker than weakly-normally graded sandstones (*fgs*) in the lower division. In addition, mudstones and sandstones above the parallel-stratified sandstone (*fps*) covering LA 8 display soft-sediment deformation structures (Fig 5b, Fig. 6b). Normally graded sandstones (*fgs*) often show evidence of erosion into the underlying intervals of LA 8. There is no clear difference in the grain size between the lower and the upper divisions.

Interpretation: The convolute structures in the upper division and chaotically distributed mud-clasts in the clast-rich muddy sandstones (*fcms*) in the upper divisions were deposited by cohesive flows. These cohesive

flow types are interpreted to have evolved from slumps in up-flow locations (Fig. 5b, Fig. 6b) (Symons *et al.,* 2016; Southern *et al.,* 2017). The fine-grained and normally graded sandstones (*fgs*) in the lower division may have been deposited by turbidity currents or concentrated flows. Such deposits indicate that some of the mass-transport divisions may have partly transformed into turbulence, deposits of which were then covered by disaggregated remnants of the slumped mass (Fig. 8b) (McCaffrey and Kneller, 2001; Haughton *et al.,* 2003; Talling, 2013).

Alternatively, the mass transport deposits induced by sediment failure may have covered preceding turbidites in the lobe-dominated part of the fan system, which in-turn led to the formation of LA 8 (Fig. 1c). Mass-transport deposits with convolute structures always accompany LA 8 (with sharp boundaries between the two deposit types) and LA 8 only develops in the slump area, jointly confirming that (according to the Walther's Law) slumping resulted in the deposition of LA 8. Parallel-stratified sandstone (*fps*), with erosional bases often rest directly above the upper divisions, which may have been deposited by ensuing sandy turbidity currents that formed through the remobilization and partial transformation of mass-transport deposits.

4.2.8 LA 9: Pebbly sandstone and muddy sandstone

Description: The thickness of LA 9 ranges from 0.3 m to 0.8 m. The lower division is composed of grey and graded pebbly sandstones (*fgps*) and the upper division is composed of muddy sandstones (*fcms*) (Fig. 7a). The lower division is composed of normally–inversely–normally graded pebbly sandstones in the lower part, and normally graded pebbly sandstone (*fgps*) with an elevated mud-matrix component in the upper part. The sedimentary characteristics of the lower and upper parts are similar to that of 'H1a' and 'H1b' sub-divisions described by Shan et al. (2019), respectively. Mud-clasts display an upward increase in both abundance and size, and water escape structures were observed in the upper part of the lower division (Fig. 7a). The lower division displays a sharp contact with underlying structureless mudstone (*fmm*). The boundary between the

lower and upper divisions is transitional. The upper division consists of muddy sandstones (*fcms*), containing small mud-clasts and phytodetritus. The grain size is finer in the upper division than compared with the upper part of the lower division. The overlying pebbly sandstones display a sharp contact with these beds and consist of normally-graded pebbly sandstones (*fgps*) in the lower portion and stratified pebbly sandstones (*fsps*) in the upper portion.

Interpretation: LA 9 is interpreted to form through particle rearrangement in debris flows. This genesis denotes that the particles above a critical size settle out preceding smaller particles within a decelerated debris flow (Fig. 8c) (*sensu* Sumner *et al.*, 2009). The floating mud-clasts and water escape structures in the coarse-grained deposits show that the upwards movement of buoyant lower-density clasts was controlled by a combination of buoyancy processes and pore pressure. The absence of a sharp boundary between the upper and lower divisions, and the vertical-stacking of the two and continuous normal grading indicate that the muddy sandstones (*fcms*) in the upper division and graded pebbly sandstones (*fgps*) in the lower division were deposited as the product of a single flow.

As the initial flow that deposited the coarse-grained deposits in the lower division (concentrated flow deposits) and muddy deposits in the upper division have a higher sediment concentration and clast-content compared to those of concentrated flow, the initial flow may have been a debris flow. In addition, the overlying graded and stratified pebbly sandstones (*fgps* and *fsps*) of LA 9 are interpreted to have formed by concentrated flows, implying that LA 9 may be the product of flow transformation from a debris flow (*sensu* Yang *et al.*, 2019). When debris flows decelerate, the rapid release of pore water leads to rearrangement of sediment particles of various sizes by remobilization or shock, with coarse sediments settling out and suspended fine sediments forming muddy sandstones (*fcms*) in the upper bed (Fig. 8c) (Baas *et al.,* 2009; Sumner *et al.,* 2009).

4.2.9 LA 10: Sandstones or siltstones with an erosional base and muddy siltstones

Description: LA 10 ranges from 0.08 m–0.15 m thick and is composed of three divisions. Fine-grained sandstones or siltstones, with an erosional base form the lower division, muddy siltstones (*fcmss*) comprise the middle division, and fine-grained sandstones with mud layers (*fps*) and overlying black mudstone (*fmm*) form the upper division (Fig. 7b). Grey siltstones containing ripple cross-lamination or parallel lamination, erosional bases, and water escape structures were observed in the lower division (Fig. 7b). The boundaries are sharp between the lower and middle divisions. The middle division has been divided into an underlying muddy siltstone (*fcmss*) with mud patches, and an overlying dark grey muddy siltstone (*fcmss*) with siltstone injections and dispersed mud (*ca* 20% to 60% visually); the sedimentary characteristics of these two divisions correspond to that of 'H3a' and 'H3b' sub-divisions as described by Dodd et al. (2022), respectively (Fig. 7b). The mud content in the middle division gradually increased upward. Brown parallel laminated siltstone (*fpss*) above the middle division, which displays parallel lamination, mud layers, laminae-scale soft-sediment deformation, as well as sharp bases, represents the 'H4'sub-division of HEBs (*sensu* Haughton *et al.*, 2009). Black mudstone caps, with dispersed very fine-grained sand and thin siltstone laminae, reflect the 'H5'sub-division of HEB. The 'H2'sub-division of HEB is absent in the LA 10, which is underlain by normally graded sandstone with parallel lamination and ripple cross lamination, and is overlain by sandstones (*fdsm*) with small-scale deformation structures (Fig. 7b).

Interpretation: LA 10 is interpreted as being deposited by sediment gravity flows that included up-dip muddy substrate erosion. The vertical staking pattern of the lower division of LA 10 and underlying turbidites show a repeated deposition of Bouma Tc and Td sediments, indicating that the deposits were formed by low-concentration turbidity currents. The erosional bases of the lower division and angular mud/sand patches in the middle division both indicate the occurrence of up-dip erosion (*sensu* Haughton *et al.,* 2003). The

injection of large mud-clasts, muddy matrix components, and vertical/longitudinal segregation processes caused by substrate erosion may have led to the formation of a quasi-laminar plug within (and/or behind) the upper turbidity current, leading to the deposition of the middle division (Fig. 8d) (Ito, 2008). The longitudinally-fractioned transformation processes of the flow, along with the flow-parallel shearing effect are interpreted to have led to the along-flow segregation of the middle division into two parts (*c.f.* Hussain et *al.*, 2020; Dodd *et al.,* 2022). The dilute turbulent wake and fallout of suspension led to the deposition of the fine-grained stratified sandstone or siltstone and mudstone cap of the upper division, respectively (Haughton *et al.,* 2009). Finally, deformed sandstones (*fdsm*) above these beds may have been induced by small flows and/or re-working by bottom currents following HEB emplacement.

4.3 Distribution of HEBs

4.3.1 Vertical organization

Gravity flow deposits are divided into progradation (presenting as funnel-shaped GR curves and upward thinning of a single mudstone interval) and retrogradation sequences (presenting as bell-shaped GR curves and upward thickening of a single mudstone interval) (Fig. 9a). HEBs are not observed within well z74-s1 in the area dominated by channel elements and characterized by amalgamated pebbly sandstones (the stacking of LA1 and LA2) and hackly boxing gamma logs (GR) (Fig. 1d, Fig. 9a). In a single well containing HEBs, the mean thickness of the HEBs accounts for approximately 15% of the total thickness of the gravity flow deposits (Fig. 9). In well z77 located in the area of the proximal lobe, the total thickness of LA 9 is thicker than that of LA 7; LA 7 associated with LA5 and LA 9 associated with LA 2 respectively form in the progradation sequence and the retrogradation sequence (Fig. 1d, Fig. 9a). In well z62 located in the area of the distal lobe, the total thickness of LA 9 associated with LA 2 is thinner than that of other HEBs (LA 7 and LA 10); LA 7 still is associated with LA5; different than in well z77, LA 10 mainly associated with LA 6 is

observed and HEBs only form in the progradation sequence except for LA 10 with the highest proportion (Fig. 1d, Fig. 9a). In the well z66-1 located in the area overlapped by slumps and distal fans, HEBs only form in the progradation sequence (Fig. 1d, Fig. 9a). Among them, LA 10 and LA 7 is mainly associating with LA6; LA 9 is not observed; and LA 8 with the highest proportion is associated with LA 4 (Fig. 9a).

Generally, LA 7 developing in progradational sequences is associated with LA5 and LA 6 respectively in areas dominated by lobes and related to slumps (Fig. 1d, Fig. 9a). LA 8 developing within progradational sequences is associated with LA 4 (Fig. 9a). LA 9 mainly developing in retrogradational sequences is observed along with LA 2 (Fig. 9a). LA 10 is observed within both the retrogradational and progradational sequences, typically displaying erosional basal contacts that always incise into mudstones (*fmm*) (Fig. 9a).

4.3.2 Lateral distribution

HEBs are observed in wells located in the area poorly related to the channel elements (Fig. 1d, Fig. 9b). HEBs with diverse origins show varied lateral distributions. In contrast with LA 7 and LA 10, the proportion of LA 9 decreases from the proximal to distal areas of the fan (Fig. 1d, Fig. 9b). In wells (z78-2, z78, z602 and z77) located in proximal lobes, LA 9 exist in higher proportions than LA 7 and LA 10, whose thickness accounts for more than 50% of the total thickness of HEBs (Fig. 1d, Fig. 9b). Among them, in wells z78-2 and z78 both situated in the area related to channel exits/mouths, LA 9 is observed along with LA 10 (Fig. 1c, Fig. 9b); in wells z602 and z77 both located in the area related to lobe margins, LA 9 is observed along with LA 7 (Fig. 1d, Fig. 9b). LA 7 is mainly observed in wells located in the area related to lobes adjacent to both sides of the channel elements or in the lobe overlap areas (Fig. 1d, Fig. 9b). The thickness of LA 7 contributes to a relatively high proportion (25.95%) of the total thickness of HEBs in well z62 related to the lobe overlap areas (Fig. 1d, Fig. 9b). LA 8 are distributed in wells z66-5 and z66-1 both situated in the area dominated by proximal slumps, and the thickness ratio of LA 8 decreases along the major transport direction

(from well z66-5 to well z66-1) (Fig. 1d, Fig. 9b). Instances of LA 10 have scattered distributions that are not clearly related to any particular position across the system surface.

4.4 Reservoir characteristics

The physical properties of gravity flow deposit reservoirs within the Es_{3L} group in the Gubei Sag exhibit pervasive heterogeneity, which is characterized by medium porosity and medium/high permeability (*c.f.* SYT/6285 − 2011). The porosity of the reservoirs ranges from 2% to 25%, mostly between 15% and 20%, and the average porosity is 17.8% (Fig. 10a). The permeability of the reservoirs ranges from 3 mD to 816 mD, mostly between 10mD and 500mD, with an average permeability ($\overline{K}$) of 126 mD and permeability ratio (R_{mn}) of 1986 (Fig. 10b). The variation coefficient of permeability (V_k) is 1.39 and heterogeneity coefficient of permeability (T_k) is 12.06.

The lateral variation in the reservoir permeability indicates that the reservoir has strong aerial/spatial heterogeneity (Fig. 10c). The lateral distribution of permeability is controlled by sedimentary facies, and the permeability of reservoirs formed by channel deposits is typically >60 mD. Five areas display low permeability (10mD to 30 mD) in the channel element areas. The permeability of reservoirs constituted by lobe deposits typically ranges from 10 mD to 60 mD. There are six circular areas within the lobes with very low permeability (<10 mD), as well as two circular areas with higher permeability (>100 mD). The reservoir permeability is typically larger in the channel element areas than compared with in the lobe elements, and reservoirs constituted by lobe deposits present stronger heterogeneity (Fig. 1c, Fig. 9c).

5. Discussion

5.1 The controlling factors of HEBs

For the discussion, LA 7, LA 8, LA 9 and LA 10 are termed HEB1, HEB2, HEB3 and HEB4 respectively,

according to their different sedimentary emplacement processes (Fig. 8). Based on the vertical organization of HEBs, LA 2, LA 5, LA 6 and LA 4 respectively indicate channels, distal channel/proximal lobe zones (channel-lobe transition zones), lobes and proximal slumps where HEBs may form (Mutti and Normark, 1987; Kane and Hodgson, 2011; Mueller *et al*., 2017; Dodd *et al*., 2019; Zavala, 2020). By combining with the locations of wells developing HEBs, it is safe to say that HEBs are typically associated with channel-lobe transition zones (CLTZs), slump proximal areas, lobe fringes, and lobe distal fringe locations in the Gubei sag. and mainly form during the initiation and growth phases of gravity flow deposits (Fig. 1d, Fig. 9). The distribution pattern of HEBs in lake settings in the Gubei Sag is similar to the results of previous studies in other areas such as the Lingshan Islands and North Falkland Basin sags (Dodd *et al.,* 2022; Yang *et al.,* 2022), and is similar to the examples from marine basins worldwide (Haughton *et al.,* 2009; Hodgson, 2009; Mueller *et al.*, 2017). The similar distribution pattern implies that the main controlling factors of HEBs in Gubei sag may be flows' concentration (Patacci et al., 2014; Patacci et al., 2020; Mansor and Amir Hassan, 2021; Jin et al., 2021). However, as opposed to marine basins, lacustrine basins are characterized by more provenances, shorter transportation distance of debris, and smaller area. Therefore, the controlling factors of HEBs in lake settings require more discussion.

During the progradational sequence, the upward thickening of concentrated flow deposits, upward thinning of black structureless sandstone (*fmm*) layers, and absence of very fine-grained caps ('H4'and 'H5') in HEB1 jointly reflect gradually enhancing transport capacity of flows (Fig. 6a, Fig. 9a). This also suggests the highest potential for increasing sand or mud content in flows, palaeotopographical interaction, and muddy substrates erosion (lead finer-grained debris to mix into flows). Consequently, increased sediment supply can act to suppress turbulence and cause transformation into cohesive flow rheologies (Baas *et al*., 2011; Fonnesu *et al.,* 2015; Mansor and Amir Hassan, 2021; Jin *et al.,* 2021). Additionally, the wells (e.g., well z62, well

z52-35 and well z66-1) showing HEB1 during the Es_{3L} times are located in the areas with thicker sedimentary thickness than their surroundings (Teng, 2016). This fact implies that the formation of HEB1 is influenced by ancient landform. In examples of HEB1 that are associated with lobe fringes and channel-lobe transition zones, palaeotopographical interaction including gully-filling and bathymetrical modification (through developing syn-depositional accommodation) may have acted to influence rheological properties of the initial flows through flow deceleration (Fig. 9b, Fig. 11e) (*sensu* Dodd *et al*., 2022). This may have in-turn resulted in rapid suspension fallout from concentrated flows and *en masse* deposition from debris flows (corresponding to the lower and upper division of HEB1, respectively). In addition, HEB1 accounts for a higher proportion in the area of superposition and intersection of lobes (higher sediment supply and stronger palaeotopographical interaction) than in any other areas, implying that terrain and sediment supply are key factors for the formation of HEB1.

This study interprets that the re-mobilization of sediments is necessary for HEB2's formation. It indicates that extrabasinal sediment supply barely controls HEB2's formation. Tectonic activities or sediment failure (at the large scale) causing sediment remobilization can change terrain or be induced by the change of terrain. And the change of terrain will lead to the change of accommodation to control the filling location of gravity flow deposits, in turn influence the distribution of HEB2 deposits. Therefore, it is inferred that the HEBs caused by slumping are mainly controlled by terrain. It is worth noting that HEBs are highly likely to be eroded and reworked during the emplacement of progradational sequences (as more proximal facies progressively migrate basin ward, they override and potentially erode into older more and distal facies of the same system), which may result in the absence of 'H4' and 'H5' divisions to form HEB1 and HEB2 with bipartite structure.

It is difficult for debris flows are difficult to erode muddy substrate, which suggests that flow

concentration and particle size hinge on the sediment supply. In retrogradational gravity flow successions, the reducing sediment supply along with lower flow energies led to flow deceleration, which in turn controlled the formation of HEB3. Decelerating debris flows with low yield strength tend to rapidly expel pore water during the process of *en masse* freezing to cause coarse-grained particles preferentially depositing and relatively fine-grained particles moving upward (i.e., particle rearrangement) (Baas et al., 2009; Cao *et al*., 2017), in turn, leads to normal settling (coarse-to-fine grained deposits from bottom to top) and deposition of the upper and lower divisions in HEB3 (Sumner *et al.*, 2009). Therefore, the HEBs caused by particle rearrangement in debris flows is regarded as being controlled by sediment supply.

In-contrast to HEB1–HEB3, the sedimentary characteristics of HEB4 indicate that a muddy substate and energetic (turbulent) flows are necessary conditions for formation (Fig. 7b) (Bell *et al.,* 2018; Jin *et al.,* 2021). HEB4's random temporal distribution denotes that its formation and distribution are likely to be barely controlled by sediment supply (Fig. 9a). Terrain can influence the flowpath of gravity flows to control the location of erosion, in turn controls the formation and distribution of the HEBs caused by erosion. And the increase of slope inclination can enhance the energy of turbulence to prompt erosion, then facilitates the formation of HEBs. In addition, the aggradation of gravity flows and the resultant modification of the lake floor sediments (deposition of sands or muds) will change the terrain and the distribution of muddy substrate to influence the formation of HEBs.

As mentioned above, terrain is the main controlling factor for HEBs induced by cohesive flows/turbidity currents; sediment supply is the main controlling factor for HEBs induced by concentrated flows/debris flows. As the particle size in flows decreases, the controlling effect of sediment supply on the formation and distribution of HEBs is weakened, with the HEBs caused by slumping being the only exception.

5.2 Sediment gravity-flow evolution processes

The lateral proportional change of different bed types (presenting the gradual reduction and cessation of LA 1, along with the increase in LA 2, LA 5, LA 6 and HEBs, moving from the source area to the depocenter) in the Gubei Sag documents the widely-recognized down-flow evolution process of a single gravity flow transitioning from a high concentration flow to a lower concentration flow during its run-out into a basin (from debris flow, to concentrated flow, to hybrid flows, and finally to turbidity currents) (Fig. 9b) (e.g., Amy and Talling, 2006; Haughton *et al*., 2009; Felix and Peakall, 2010; Lowe *et al*., 2010; Talling *et al*., 2013; Pickering and Hiscott, 2015; Southern *et al.,* 2015; Dodd *et al.,* 2022; Yang *et al.,* 2022). Different HEB types form in progradation or/and retrogradation sequences, which may suggest a longitudinal HEB evolution pattern from HEB1/HEB2 to HEB3 (Fig. 9a). The temporal and spatial distribution pattern of HEBs, and their complex lithofacies associations suggest that different HEB types have specific sedimentary evolution processes (Fig. 11).

Three HEB types (HEB1, HEB3 and HEB4) form in the subaqueous fans. Instances of HEB1 and HEB4 observed within the lobe are interpreted to have formed through the partial transformation of turbulence and are associated with turbidities (Fig. 8a, Fig. 8d, Fig. 11e). The sedimentary pattern of HEB1 and HEB4 suggests that HEB1 and HEB4 form during the sedimentary process from concentrated flow deposits to turbidity current deposits (Fig. 11a, 11c). HEB1s are only involved in the sedimentary evolution stage of subaqueous fan's expansion according to their temporal distribution (Fig. 11a). HEB4s form both in progradation and retrogradation sequences, suggesting that HEB4 can be involved in various evolution stages of subaqueous fan, but do not indicate that there is any longitudinal evolution pattern between HEB1 and HEB4. However, in these examples it is possible that less mud is incorporated into flows that would otherwise help promote flow transformation; it is possible that this would limit HEB4 development during

retrogradational phases of the fan. HEB3s are mainly involved in the sedimentary evolution stage of subaqueous fan's back-stepping. As HEB3s are typically formed in retrogradation sequences associated with LA 2, and the lower and upper divisions are produced by debris flow, the HEB3 are interpreted as forming before concentrated flow deposition according to the widely-recognized evolution process of gravity flow (Fig. 11b) (Yang *et al.,* 2019). This further validates the sedimentary model whereby the debris flow of HEB3 transformed into concentrated flows in down-flow areas (Fig. 11b). It is noted that the formation process of HEB3s does not include flow transformation. Therefore, HEB3s is just a product of debris flows along with the decreasing of flow concentration and weakening of energy. HEB3s accounts for as a higher proportion than HEB1 in proximal lobe element areas, denoting the spatial evolution from HEB3 to HEB1. Based on the comprehensive analysis of the results, the sedimentary evolution process of gravity flows in the sedimentary system of subaqueous fans can be summarized as follows: debris flows, debris flows with lower concentration (than initial debris flows) that lead to the formation of HEB3, and the formation of HEB1and HEB4 that can form during the sedimentary evolution process from concentrated flows to turbidity currents in the distal areas.

slumps are considered outwith this overall high concentration to low concentration sediment gravity flow model, largely as they are more local features that are induced by the slumping of fan deposits, most commonly in distal or fringing areas of the system (Fig. 1d, Fig. 11e). In the oval area associated with slumps, the proportion of LA 4 decreases whereas the proportion of LA5 and LA6 from proximal area to distal area increase, and besides HEBs only LA6 caused by turbidity currents is observed in well z23-2 located at the tail end of slumps (Fig. 9b), both of which reflect the transformation from cohesive flows into turbulences. As the slump began to accelerate and deform, turbidity current may be generated through the process of sediments being eroded from the slump toe and upper surface by ambient fluid-driven shear or surface

transformation. (Strachan, 2010). HEB1, HEB2 and HEB4 are observed to be spatially and temporally associated with slump deposits. With the proportion of LA 4 decreasing, the proportion of HEB2 decreases (Fig. 9b). Therefore, HEB2 tend to be observed within the proximal slump areas and are interpreted to be associated with the transformation of the slump-related mass-transport flows into lower concentration flows (flow transformation) (Fig. 11d). As opposed to HEB2, HEB1 and HEB4 are far from the starting end of slumps (Fig. 1d, Fig. 9b), which reveals that HEB4 and HEB1 form after HEB2 during transportation. The uniformity of lateral proportional change of LA5 and HEB1 as well as LA6 and HEB4 also reveals that HEB4 and HEB1 form during the sedimentary evolution process from concentrated flows to turbidity currents (Fig. 9b, Fig. 11d).

5.3 The influence of HEBs on deep-lacustrine fan reservoir heterogeneity

Although sedimentologists have judged that the existence of HEBs can affect the reservoir heterogeneity in deep-marine fan systems (e.g., Mueller *et al.,* 2017; Spychala *et al.,* 2017), there is currently comparatively less evidence to show how HEBs directly impact heterogeneity and reservoir parameters in deep-lacustrine fan systems (e.g., Dodd *et al.*, 2022; Yang *et al.,* 2022). Moreover, there is little evidence from production data through a deep-lacustrine reservoir that documents the impact of HEBs on production over the lifetime of a single field. The effects of HEBs on heterogeneity and production from a deep-lacustrine gravity flow deposits reservoir are shown in this study, which is therefore valuable to other researchers and industry, alike.

This study demonstrates that HEBs control reservoir properties within deep-lacustrine fan reservoirs. Firstly, the existence of HEBs leads to decreased permeability of reservoir zones in which they are deposited. The average permeability ($\overline{K}$) of the reservoir in well z66-1 (7.64 mD) is much lower than those in well z66-4 (185.33 mD) and well z66-12-12 (70.58 mD) adjacent to well z66-1 (Fig. 12). Areas with the lowest permeability ($\overline{K}$ < 10 mD) are formed around wells with HEBs (Fig. 9b, Fig. 10c). The morphology of the

low-permeability area is consistent with the lateral distribution characteristics of HEBs, supporting the strong correlation between the low permeability and HEBs.

Secondly, HEB formation enhances reservoir heterogeneity. The R_{mn}, V_k, and T_k of the reservoirs in well z66-4 and well z66-12-12 are much smaller than those of the reservoir with HEBs in well z66-1 (Fig. 12). The R_{mn} of 1545.61, V_k of 1.34, and the T_k of 10.05 indicate strong heterogeneity in the reservoir comprising HEBs and lacustrine gravity flow deposits in well z66-1. Notably, heterogeneous proximal lobe deposition with deformation can lead to the formation of HEB2 with relatively weak heterogeneity (compared with other HEB types) and low permeability. As opposed to the sedimentary beds without HEBs in wells z66-4 and z66-12-12, the R_{mn} (3.3 and 15.33), V_k (0.39 and 0.62) and T_k (1.90 and 2.38) of sedimentary beds with HEB2 do not clearly increase in well z66-1 (Fig. 12). The R_{mn} (877.52), V_k (1.19), and T_k (7.73) of sedimentary beds between 3398 m to 3411 m with HEB1 and HEB4 are much larger than those of the sedimentary beds with HEB2. Laterally, the oval-shaped area of the HEB deposition with low permeability enhances reservoir heterogeneity, thus increasing the difficulty in optimizing the well pattern design. Deposits with high mud content in HEBs lead to an increased quantity and thickness of interlayers, which can further increase reservoir heterogeneity and development difficulties.

Finally, during the initial stages of oil field development, the water cut of reservoirs without HEBs in z66-4 is 5.5%, whereas the water cut of the reservoir with HEBs in well z66-5 and in well 66-1 are 80.8% and 46.2%, respectively (at the same depth). The difference in the reservoir water cut in the initial development stage between lacustrine gravity flow deposits with and without HEBs suggests that HEBs control hydrocarbon and/or fluid migration and accumulation. Additionally, in the water injection stages of development, water breakthrough occurs in well z66-1, and the recovery ratio of well z66-12-12 and well z66-4 is improved. As opposed to well z66-1, wells z66-12-12 and z66-4 both have weak vertical

heterogeneity. In the intervals with HEBs of well z66-1, the porosity and permeability at the bottom of HEBs are the highest and decrease upward (Fig. 12), suggesting that the moving upward of mud debris and the formation of clean sandstones can result in strong vertical heterogeneity. Compared with the porosity and permeability of intervals with HEBs, intervals without HEBs always exhibit higher porosity and permeability in well z66-1 (Fig. 12), which further increases vertical heterogeneity. Vertically, the permeability differences within intervals with HEBs as well as between intervals with and without HEBs may make injected water stream in clean sandstones with relatively high permeability, and contribute to the occurrence of water breakthrough. Therefore, based on the analyses of reservoir properties, it is concluded that the presence of HEBs is the main factor leading to water breakthrough.

In general, the presence of HEBs increases the bulk heterogeneity within gravity flow reservoirs and reduces the mean permeability of reservoirs. Therefore, the distribution and characteristics of HEBs should always be considered during reservoir modelling and well plan optimization phases of hydrocarbon field development.

6. Conclusions

(1) Four types of HEBs in lake setting are observed, exhibiting incomplete stacking of HEB sub-divisions (H1 to H5). Bipartite HEB1, characterized by clast-poor siltstones in the upper division, are interpreted to be produced by flow transformation via relative buoyancy of lower-density debris flows. HEB2 is associated with slumping and contains thickly-bedded muddy sandstones, with convolute structures in the upper division. The examples of the pebbly sandstone-rich bipartite HEB3 are interpreted to be formed by the rearrangement of debris flow particles. HEB4’s formation is attributed to muddy substrate erosion by turbidity currents and presents stratified sandstone and a bi-partite structure in the lower and middle divisions, respectively.

(2) HEB1 and HEB4 form in distal area, and HEB2 and HEB3 form in proximal area. The lateral proportional change of different bed types reveals that HEB2 and HEB3 respectively deposit after *en masse* freezing of cohesive flows and debris flows, and HEB1 and HEB4 both form during the sedimentary evolution process from concentrated flows to turbidity currents. Sediment supply and terrain are main controlling factor for the formation and distribution of lacustrine HEBs.

(3) The consistency of low permeability (<10 mD) area and HEBs' distribution reveals that HEBs form non-reservoir divisions and lead to decreased volume and occurrence of interbeds as well as strong reservoir heterogeneity. High water cut of reservoirs during the initial stages of development and the occurrence of water breakthrough in wells with HEBs respectively reveal that HEBs may be related to hindered hydrocarbon migration and accumulation (i.e., charge issues) and has negative effect on hydrocarbon development.

Declaration of competing interest

The authors declare that they have no known competing interests that could have appeared to influence the work reported in this paper.

Acknowledgements

We are indebted to the Editor Prof. Massimo Moretti and the anonymous reviewer for their insightful comments and suggestions that have greatly improved the manuscript. This work is supported by the National Science and Technology Major Project (Grant No. 2016ZX05033). Our thanks go to the Shengli Oilfield Company of the SINOPEC Group for their support in sample collection and rock core observation. This paper is published by permission of the Executive Director, British Geological Survey (UKRI).

Data Availability

Data will be made available on request.

References

Amy, L.A., Talling, P.J., 2006. Anatomy of turbidites and linked debrites based on long distance (120 x 30 km) bed correlation, Marnoso Arenacea Formation, Northern Apennines, Italy. Sedimentology, 53, 161–212.

Amy, L.A., Peachey, S.A., Gardiner, A.A., Talling, P.J. 2009. Prediction of hydrocarbon recovery from turbidite sandstones with linked-debrite facies: Numerical flow-simulation studies. Marine and Petroleum Geology, 26, 2032–2043.

Baas, J.H., Best, J.L., Peakall, J., 2011. Depositional processes, bedform development and hybrid bed formation in rapidly decelerated cohesive (mud-sand) sediment flows. Sedimentology 58, 1953-1987.

Baas, J.H., Best, J.L., Peakall, J., Wang, M., 2009. A Phase Diagram for Turbulent, Transitional, and Laminar Clay Suspension Flows. Journal of Sedimentary Research 79, 162-183.

Baas, J.H., Tracey, N.D., Peakall, J., 2021. Sole marks reveal deep-marine depositional process and environment: implications for flow transformation and hybrid-event-bed models. Journal of Sedimentary Research 91, 986-1009.

Baker, M.L., Baas, J.H., 2020. Mixed sand-mud bedforms produced by transient turbulent flows in the fringe of submarine fans: Indicators of flow transformation. Sedimentology 67, 2645-2671.

Bell, D., Kane, I.A., Pontén, A.S. M., Flint, S.S., Hodgson, D.M., Barrett, B.J., 2018. Spatial variability in depositional reservoir quality of deep-water channel-fill and lobe deposits. Marine and Petroleum Geology 98, 97-115.

Bell, D., Stevenson, C.J., Kane, I.A., Hodgson, D.M., Poyatos-More, M., 2018. Topographic controls on the development of contemporaneous but contrasting Basin-floor depositional architectures. Journal of

Sedimentary Research 88, 1166-1189.

Bouma, A.H., 1962. Sedimentology of Some Flysh Deposits: A Graphic Approach to Facies Interpretation. Elsevier, Amsterdam, 168 pp.

Cao, Y., Yang, T., Wang. Y., 2017. Types and genesis of deep-water hybrid event beds comprising debris flow and turbidity current. Earth Science Frontiers 24, 234-248 (in Chinese with English abstract).

Davis, C., Haughton, P., McCaffrey, W., Scott, E., Hogg, N., Kitching, D., 2009. Character and distribution of hybrid sediment gravity flow deposits from the outer Forties Fan, Palaeocene Central North Sea, UKCS. Marine and Petroleum Geology 26, 1919-1939.

Dodd, T.J.H., McCarthy, D.J., Richards, P.C., 2019. A depositional model for deep-lacustrine, partially confined, turbidite fans; Early Cretaceous, North Falkland Basin. Sedimentology 66, 53-80.

Dodd, T.J.H., McCarthy, D.J., Amy, L., Plenderleith, G.E., Clarke, S.M., 2022. Hybrid event bed character and distribution in the context of ancient deep-lacustrine fan models. Sedimentology 69, 1891-1926.

Felix, M., Peakall, J., 2010. Transformation of debris flows into turbidity currents: mechanisms inferred from laboratory experiments. Sedimentology 53, 107-123.

Felix, M., Leszczynski, S., Slaczka, A., Uchman, A., Amy, L., Peakall, J., 2009. Field expressions of the transformation of debris flows into turbidity currents, with examples from the Polish Carpathians and the French Maritime Alps. Marine and Petroleum Geology 26, 2011-2020.

Fonnesu, M., Haughton, P., Felletti, F., McCaffrey, W., 2015. Short length-scale variability of hybrid event beds and its applied significance. Marine and Petroleum Geology 67, 583-603.

Fonnesu, M., Patacci, M., Haughton, P.D.W., Felletti, F., McCaffrey, W.D., 2016. Hybrid Event Beds Generated by Local Substrate Delamination on A Confined-Basin Floor. Journal of Sedimentary Research 86, 929-943.

Ge, Z., Nemec, W., Vellinga, A.J., Gawthorpe, R.L., 2022. How is a turbidite actually deposited? Science advances

8, eabl9124. https:// doi.org/10.1126/sciadv.abl9124.

Girard, F., Ghienne, J.F., Rubino, J.L., 2012. Occurrence of Hyperpycnal Flows and Hybrid Event Beds Related to Glacial Outburst Events in A Late Ordovician Proglacial Delta (Murzuq Basin, SW Libya). Journal of Sedimentary Research 82, 688-708.

Grundvag, S.A., Johannessen, E.P., Helland-Hansen, W., Plink-Bjorklund, P., 2014. Depositional architecture and evolution of progradationally stacked lobe complexes in the Eocene Central Basin of Spitsbergen. Sedimentology 61, 535-569.

Haughton, P., Barker, S.P., Mccaffrey, W.D., 2003. 'Linked' debrites in sand‐rich turbidite systems – origin and significance. Sedimentology 50, 459-482.

Haughton, P., Davis, C., McCaffrey, W., Barker, S., 2009. Hybrid sediment gravity flow deposits – Classification, origin and significance. Marine and Petroleum Geology 26, 1900-1918.

Hodgson, D.M., 2009. Distribution and origin of hybrid beds in sand-rich submarine fans of the Tanqua depocentre, Karoo Basin, South Africa. Marine and Petroleum Geology 26, 1940-1956.

Hussain, A., Haughton, P.D.W., Shannon, P.M., Turner, J.N., Pierce, C.S., Obradors-Latre, A., Barker, S.P. Martinsen, O.J., 2020. High-resolution X-ray fluorescence profiling of hybrid events: Implications for sediment gravity flow behaviour and deposit structure. Sedimentology, 67, 2850–2882.

Ito, M., 2008. Down fan Transformation from Turbidity Currents to Debris Flows at a Channel-to-Lobe Transitional Zone: The Lower Pleistocene Otadai Formation, Boso Peninsula, Japan. Journal of Sedimentary Research 78, 668-682.

Jackson, A.L., Zakaria, A.A., Johnson, H.D., Tongkul, F., Crevello, P.D., 2009. Sedimentology, stratigraphic occurrence and origin of linked debrites in the West Crocker Formation (Oligo-Miocene), Sabah, NW Borneo. Marine and Petroleum Geology 26, 1957-1973.

Jin, L., Shan, X., Shi, X., Fonnesu, M., Qiao, S., Kandasamy, S., Wang, H., Liu, S., Fang, X., Zou, X., 2021. Hybrid event beds generated by erosional bulking of modern hyperpycnal flows on the Choshui River delta front, Taiwan Strait. Sedimentology 68, 2500-2522.

Kane I.A., Hodgson D.M., 2011. Sedimentological criteria to differentiate submarine channel levee Subenvironments: exhumed examples from the Rosario FM. (upper Cretaceous) of Baja California, Mexico, and the Fort Brown FM Permian), Karoo Basin, S. Africa. Marine and Petroleum Geology 28, 807-823.

Kane, I.A., Pontén, A.S.M., 2012. Submarine transitional flow deposits in the Paleogene Gulf of Mexico. Geology, November, 2012. https://doi:10.1130/G33410.1

Li, T., Jiang, Z., Xu, C., Yuan, Y., Wang., P., Liu, G., Zhang, B., Ning, C., Wang, Zhi, 2017. Effect of sedimentary environment on shale lithofacies in the lower third member of the Shahejie Formation, Zhanhua Sag, eastern China. 5, T487-T501.

Liu, F., Zhu, X., Li, Y., Xue, M., Sun, J., 2016. Sedimentary facies analysis and depositional model of gravity-flow deposits of the Yanchang Formation, southwestern Ordos Basin, NW China. Australian journal of earth sciences 63, 885-902.

Liu, J., Xian, B., Wang, J., Ji, Y., Lu, Z., Liu, S., 2017. Sedimentary architecture of a sub-lacustrine debris fan: Eocene Dongying Depression, Bohai Bay Basin, east China. Sedimentary Geology 362, 66-82.

Liao, J., 2021. Oil Layer Correlation and sedimentary Facies Analysis of the Oil Group I of the lower Es3 in Gubei Sag (M.Sc. thesis). China University of Geosciences (Beijing), 80 pp (in Chinese with English abstract).

Lowe, D.R., 1976. Subaqueous liquefied and fluidized sediment flows and their deposits. Sedimentology 23, 285-308.

Lowe, D.R., 1982. Sediment gravity flows; II, Depositional models with special reference to the deposits of high-density turbidity currents. Journal of sedimentary petrology 52, 279-297.

Lowe, D.R., Guy, M., 2000. Slurry-flow deposits in the Britannia Formation (Lower Cretaceous), North Sea; a new perspective on the turbidity current and debris flow problem. Sedimentology 47, 31-70.

Lowe, D.R., Guy, M., Palfrey, A., 2010. Facies of slurry‐flow deposits, Britannia Formation (Lower Cretaceous), North Sea: implications for flow evolution and deposit geometry. Sedimentology 50, 45-80.

Mansor, H.E., Amir Hassan, M.H., 2021. Facies and bed type characteristics of channel‐lobe transition deposits from the Oligocene–Miocene Tajau Sandstone Member, Kudat Formation, Sabah, Malaysia. Geological Journal 56, 5642-5672.

Mattern, F., 2005. Ancient sand-rich submarine fans: depositional systems, models, identification, and analysis. Earth-science reviews 70, 167-202.

McCaffrey, W., Kneller, B., 2001. Process controls on the development of stratigraphic trap potential on the margins of confined turbidite systems and aids to reservoir evaluation. AAPG bulletin 85, 971-988.

Middleton, G.V., Hampton, M.A., 1973. Sediment gravity flows: mechanics of flow and deposition. In: Middleton, G.V., Bouma, A.H. (Eds), Short course notes, Pacific Section of The Society of Economc Paleontologists and Mineralogists, Turbidites and Deep-Water Sedimentation, pp. 1–38.

Muskat, M., 1937. The Flow of Homogeneous Fluids through Porous Media. Mcgraw-Hill Book Company Inc, New York and London, 110 − 113 pp.

Mulder, T., Alexander, J., 2001. The physical character of subaqueous sedimentary density flows and their deposits. Sedimentology 48, 269-299.

Mutti, E., Normark, W.R., 1987. Comparing examples of modern and ancient turbidite systems: problems and concepts. In: Leggett, J.K., Zuffa, G.G. (Eds.), Marine Clastic Sedimentology: Concepts and Case Studies. Graham & Trotman, Oxford, pp. 1–38.

Mutti, E., Tinterri, R., Benevelli, G., Biase, D.D., Cavanna, G., 2003. Deltaic, mixed and turbidite sedimentation

of ancient foreland basins. Marine and Petroleum Geology 20, 733-755.

Mueller, P., Patacci, M., Di Giulio, A., 2017. Hybrid event beds in the proximal to distal extensive lobe domain of the coarse-grained and sand-rich Bordighera turbidite system (NW Italy). Marine and Petroleum Geology 86, 908-931.

Patacci, M., Haughton, P.D.W., McCaffrey, W.D., 2014. Rheological complexity in sediment gravity flows forced to decelerate against a confining slope, Braux, SE France. Journal of Sedimentary Research, 84, 270–277.

Patacci, M., Marini, M., Felletti, F., Di, G.A., Setti, M., McCaffrey, W., 2020. Origin of mud in turbidites and hybrid event beds: Insight from ponded mudstone caps of the Castagnola turbidite system (north‐west Italy). Sedimentology 67, 2625-2644.

Pickering, K., Stow, D., Watson, M., Hiscott, R., 1986. Deep-water facies, processes and models: a review and classification scheme for modern and ancient sediments. Earth-Science Reviews 23, 75-174.

Pickering, K.T., Hiscott, R.N., 2015. Deep Marine Systems: Processes, Deposits, Environments, Tectonics and Sedimentation. John Wiley & Sons, American, 656 pp.

Pierce, C.S., Haughton, P.D.W., Shannon, P.M., Pulham, A.J., Barker, S.P., Martinsen, O.J., 2018. Variable character and diverse origin of hybrid event beds in a sandy submarine fan system, Pennsylvanian Ross Sandstone Formation, western Ireland. Sedimentology 65, 952-992.

Piper, D., Normark, W.R., 2009. Processes That Initiate Turbidity Currents and Their Influence on Turbidites: A Marine Geology Perspective. Journal of Sedimentary Research 79, 347-362.

Postma, G., 1986. Classification for sediment gravity-flow deposits based on flow conditions during sedimentation. Geology 14, 291-294.

Pritchard, D., Gladstone, C., 2009. Reversing buoyancy in turbidity currents: developing a hypothesis for flow transformation and for deposit facies and architecture. Marine and Petroleum Geology 26, 1997-2010.

Shanmugam, G., 2000. 50 years of the turbidite paradigm (1950s—1990s): deep-water processes and facies models—a critical perspective. Marine and Petroleum Geology 17, 285-342.

Shanmugam, G., 2013. New perspectives on deep-water sandstones: Implications. Petroleum Exploration and Development 40, 316-324.

Shan, X., Yu, X.H., J, L.N., Tan, C.P., Li, S.L., Wang, J.H., 2021. Bed type and flow mechanism of deep water sub-lacustrine fan fringe facies: an example from the Middle Permian Lucaogou Formation in Southern Junggar Basin of NW China.Petroleum Science 18, 339-361.

Sohn, Y.K., 1997. On traction-carpet sedimentation. Journal of Sedimentary Research 67, 502–509.

Southern, S.J., Kane, I.A., Warchoł, M.J., Porten, K.W. and McCaffrey, W.D., 2017. Hybrid event beds dominated by transitional-flow facies: character, distribution and significance in the Maastrichtian Springar Formation, north-west Vøring Basin, Norwegian Sea. Sedimentology 64, 747-776.

Spychala, Y.T., Hodgson, D.M., Lee, D.R., 2017. Autogenic controls on hybrid bed distribution in submarine lobe complexes. Marine and Petroleum Geology 88, 1078-1093.

Spychala, Y.T., Hodgson, D.M., Prélat, A., Kane, I.A., Flint, S.S., Mountney, N.P., 2017. Frontal and Lateral Submarine Lobe Fringes: Comparing Sedimentary Facies, Architecture and Flow Processes. Journal of Sedimentary Research 87, 75-96.

Strachan, L. J., 2010, Flow transformations in slumps: a case study from the Waitemata Basin, New Zealand. Sedimentology 55(5), 1311-1332.

Sumner, E.J., Talling, P.J., Amy, L.A., 2009. Deposits of flows transitional between turbidity current and debris flow. Geology 37, 991-994.

Symons, W.O., Sumner, E.J., Talling, P.J., Cartigny, M.J.B., Clare, M.A., 2016. Large-scale sediment waves and scours on the modern seafloor and their implications for the prevalence of supercritical flows. Marine

Geology 371, 130-148.

Shi, S. 2016. Turbidite Channel Sandbody Prediction and Lithologic Reservoir Exploration in Gubei Sag. Special Oil & Gas Reservoirs 23, 16-20 (in Chinese with English abstract).

Shi, W., Zhao, W., 2003. Sedimentary characteristics of fan-deltaic depositional system in the third member of Shahejie formation in Gubei oil field. Journal-University of Petroleum China Natural Science Edition 27, 15-18 (in Chinese with English abstract).

Talling, P.J., 2013. Hybrid submarine flows comprising turbidity current and cohesive debris flow: Deposits, theoretical and experimental analyses, and generalized models. Geosphere 9, 460-488.

Talling, P.J., Amy, L.A., Wynn, R.B., Peakall, J., Robinson, M., 2004. Beds comprising debrite sandwiched within co-genetic turbidite: origin and widespread occurrence in distal depositional environments. Sedimentology 51, 163-194.

Talling, P.J., Wynn, R.B., Masson, D.G., Frenz, M., Cronin, B.T., Schiebel, R., Akhmetzhanov, A.M., Dallmeier-Tiessen, S., Weaver, P. P. E., Georgiopoulou, A., Zühlsdorff, C., Amy, L.A., 2007. Onset of submarine debris flow deposition far from original giant landslide. Nature 450, 541-544.

Talling, P.J., Masson, D.G., Sumner, E.J., Malgesini, G., 2012. Subaqueous sediment density flows: Depositional processes and deposit types. Sedimentology 59, 1937-2003.

Talling, P.J., Paull, C.K., Piper, D.J., 2013. How are subaqueous sediment density flows triggered, what is their internal structure and how does it evolve? Direct observations from monitoring of active flows. Earth-science reviews 125, 244-287.

Teng, B., 2016. The sedimentary Characteristics and Reservoir forming Law in the 9th Member of lower Es3 Formation in Gubei sag (M.Sc. thesis). China University of Petroleum (East China), 67 pp (in Chinese with English abstract).

Tan, M., Zhu, X., Geng, M., Liu, C., 2016. The Flow Transforming Deposits of Sedimentary Gravity Flow-Hybrid Event Bed. Acta Sedimentologica Sinica 34, 1108-1119 (in Chinese with English abstract).

Xian, B.Z., Wang, J.H., Liu, J.P., Dong, Y.L., Gong, C.L., Lu, Z.Y., 2018. Delta-fed turbidites in a lacustrine rift basin: the Eocene Dongying depression, Bohai Bay Basin, East China. Australian Journal of Earth Sciences 65, 135-151.

Yang, T., Cao, Y., Friis, H., Liu, K., Wang, Y., 2018. Origin and evolution processes of hybrid event beds in the Lower Cretaceous of the Lingshan Island, eastern China. Australian Journal of Earth Sciences 65, 517-534.

Yang, T., Cao, Y., Liu, K., Wang, Y., Zavala, C., Friis, H., Song, M., Yuan, G., Liang, C., Xi, K., Wang, J., 2019. Genesis and depositional model of subaqueous sediment gravity-flow deposits in a lacustrine rift basin as exemplified by the Eocene Shahejie Formation in the Jiyang Depression, Eastern China. Marine and Petroleum Geology 102, 231-257.

Yang, T., Cao, Y., Liu, K., Tian, J., Kneller, B., 2022. Depositional elements and evolution of gravity-flow deposits on Lingshan Island (Eastern China): An integrated outcrop-subsurface study. Marine and Petroleum Geology 138, 105566.

Zavala, C., 2020. Hyperpycnal (over density) flows and deposits. Journal of Palaeogeography 9, 1-21.

Zavala, C., Arcuri, M., 2016. Intrabasinal and extrabasinal turbidites: Origin and distinctive characteristics. Sedimentary Geology 337, 36-54.

Zavala, C., Pan, S., 2018. Hyperpycnal flows and hyperpycnites: Origin and distinctive characteristics. Lithologic Reservoirs 30, 1-27.

Zhao, C., 2007. Fracture features of Guantao to Dongying Formation in Zhuangnan fault zone, Gubei Subsag. Petroleum Geology and Recovery Efficiency 1, 50-51 (in Chinese with English abstract).

Zhuang, W., Fang, X., Yang, X., 2003. Geologic feature and reservoir forming pattern of Shahejie formation in

Gubei sag. Special Oil & Gas Reservoirs 2, 34-37 (in Chinese with English abstract).

Zhang, J., Ling, C., Zheng, H., 2002. Controlling action of fractures, palaeogeomorphology and material sources of rift lake basin on sedimentary system-taking Es3 Gubei subsag as example. Petroleum Geology and Recovery Efficiency 4, 24-27 (in Chinese with English abstract).

Zhang, Z., Wang, H., 2023, Sedimentary Characteristics and Depositional Model of Lacustrine Gravity Flows: A Case Study of Paleogene Shahejie Formation in the Gubei Sag, Eastern China. Lithosphere 2023 (1): lithosphere_2023_187. https://doi.org/10.2113/2023/lithosphere_2023_187.

Table. 1 Lithofacies scheme developed for this study. The facies codes, titles, descriptions, and interpretations of associated sedimentary process of emplacement for each facies have been provided.

Facies code	Facies title	Description	Interpretation
fmps	Structureless pebbly sandstone	Medium- to coarse-grained, poorly-sorted, rounded or sub-rounded, grey pebbly sandstone, with loaded bases (Fig. 3a). Mudstones typically occur directly above this lithofacies. Dispersed filamentous	An abrupt deposition of the pebble-sand mixture below a concentrated flow (Pickering and Hiscott, 2015); alternatively, the *en masse* freezing of a debris flow (Lowe, 1982).
fgps	Graded pebbly sandstone	Fine- to coarse-grained, poorly- to well-sorted, grey, sub-rounded to rounded, normally graded, or inversely graded pebbly sandstone. Occasionally, normally graded pebbly sandstone displays erosional bases (Fig. 4). Normally graded and inversely graded pebbly	Rapid vertical suspension fallout from a concentrated flow (Lowe, 1982; Pickering and Hiscott, 2015). Alternatively, when examples of inversely-then-normally graded pebbly sandstones are observed, these deposits may indicate deposition from a
fsps	Stratified pebbly sandstone	Alternations of pebble layers and sand-rich layers, which have a spacing that ranges from 1 cm to 3 cm (Fig. 4a). The pebble layers comprise sub-angular to sub-rounded gravels and the sand-rich	This facies mainly forms through grain-by-grain deposition caused by suspension and bed load traction transport by concentrated flows (Pickering and Hiscott, 2015).
fms	Structureless sandstone	Grey colored, fine- to medium-grained, well-sorted sandstone (Fig. 3b). Occasional dark grey mud layers or clasts are dispersed at the top (Fig. 5a). This facies forms stacked and amalgamated packages	This facies is interpreted to have formed by the rapid deposition under a concentrated sediment gravity flow (e.g., a high-density turbidity current), or through *en masse* freezing of a sandy

fgs	Normally graded sandstone	Fine- to coarse-grained, moderate- to well-sorted, grey, normally graded sandstone. Normally graded sandstones display a coarse-grained base (Fig. 5c). Occasional dark grey mud layers are observed	Sand suspension fall-out of concentrated flows or deposition underneath a rapidly decelerated turbidity current (Pickering and Hiscott, 2015).
fps	Parallel-stratified sandstone	Fine-grained, well-sorted, parallel laminated, normally graded sandstone (Fig. 5c).	This facies is directly equivalent to the Tb interval of the Bouma sequence, and so is interpreted to be the product of
frxbs	Ripple cross-bedded sandstone (or siltstone)	Fine-grained, well-sorted, dark grey ripple cross-laminated sandstone and/or siltstone (Fig. 5c). The ripple cross laminae display argillaceous silt-grade drapes on individual foresets and on bounding	This facies is similar to the Tc interval of the Bouma sequence, and so is interpreted to be the product of a decelerating low-density turbidity current (Bouma, 1962). Alternatively, these
fdsm	Deformed sandstone and	Plastic deformation of a complex sand-mud mix, with discrete internal glide or shear surfaces (Fig. 5b). Upper and lower bounding	Sediment remobilization through sediment failure, or gravity flow erosion that gave rise to the formation of the deformed
fcms	Muddy sandstone	Structureless, poorly-sorted, brown, fine- to coarse-grained, clast-rich sandstone (Fig. 3b). Clasts mainly consist of elongate, angular, black-grey, sometimes armored mud-clasts, lithic fragments, and filamentous carbonaceous fragments. The mud-clasts and	This facies is interpreted as being deposited through *en masse* freezing of a cohesive flow (Pickering and Hiscott, 2015). Sandstones that are absent of elongate mud-clasts indicate rapid deposition of the grains in a concentrated flow (Baas *et al.,*
fcmss	Muddy siltstone	Structureless, well-sorted, matrix-supported dark grey siltstone with dispersed clasts (Fig. 3e). Clasts consists of rounded mud-clasts, mud patches, and carbonaceous fragments. The size of mud-clasts in	Rapid suspension fallout from concentrated flow (Lowe, 1982). *En masse* deposition in cohesive flows (Haughton *et al*., 2009).

fmss	Structureless siltstone	Grey, well-sorted, structureless or weakly normally graded siltstone that lack erosional features at the base (Fig. 3d). Dispersed flecks and detritus are observed.	Structureless siltstones are likely to be transported by silt-laden concentrated flows (Talling, 2013). Dispersed flecks and detritus indicate *en masse* deposits from a plastic flow,
fpss	Parallel laminated siltstone	Well-sorted, parallel-laminated, dark grey siltstone. Mud layers are occasionally observed at the top.	Turbidity currents triggering suspension of silt and fine-grained material in flows, followed by uniform settling of silts and other fine-grained material, leading to the parallel lamination
fmm	Structureless mudstone	Dark grey to black structureless mudstone, with sharp upper and lower boundaries (Fig. 3f). Dispersed very fine-grained sand and	The deposition of suspended mud in deep lake or an abrupt freezing of fluid-mud (Baas *et al*., 2011; Talling *et al*, 2012).

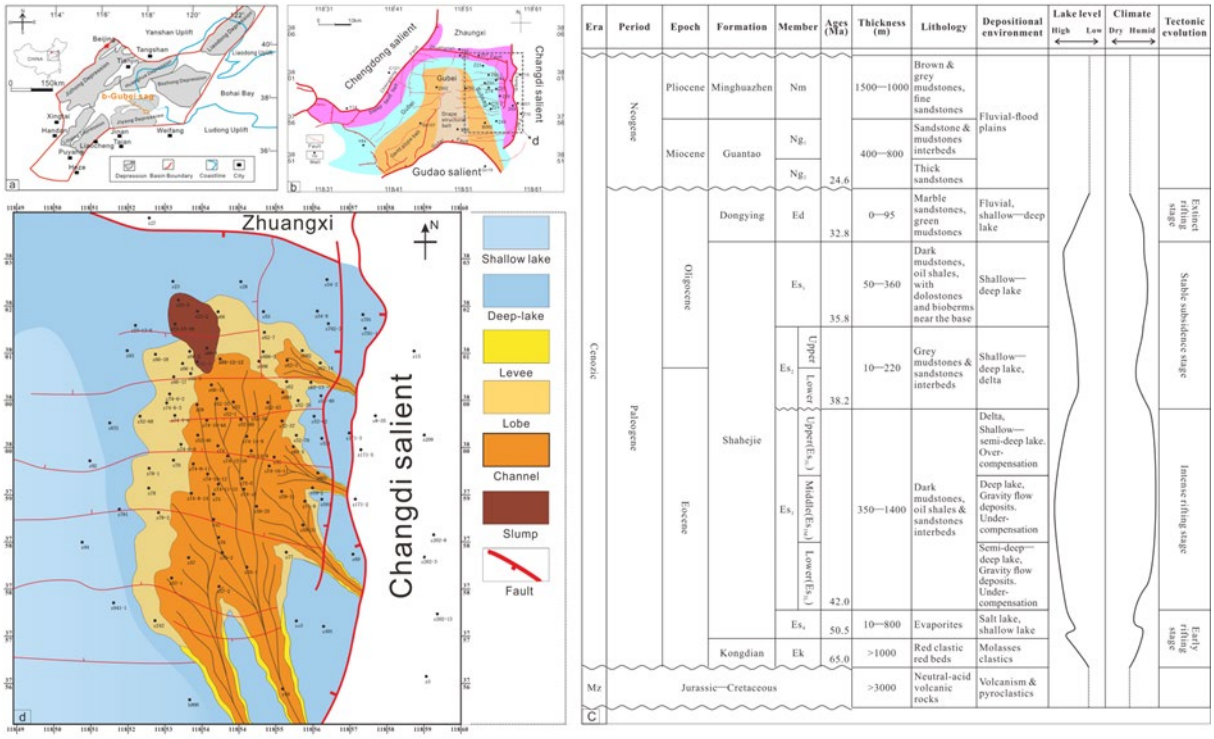

Figure 1. Image displaying (a) location of the Bohai Bay Basin; (b) simplified geologic map of the Gubei Sag; (c) stratigraphic units (age, thickness, sedimentary features, depositional setting, lake level changes, climate changes and tectonic evolution) in the Gubei Sag; and (d) distribution pattern of sedimentary facies in the third member of Shahejie formation (Es_3) (after Zhang and Wang, 2023).

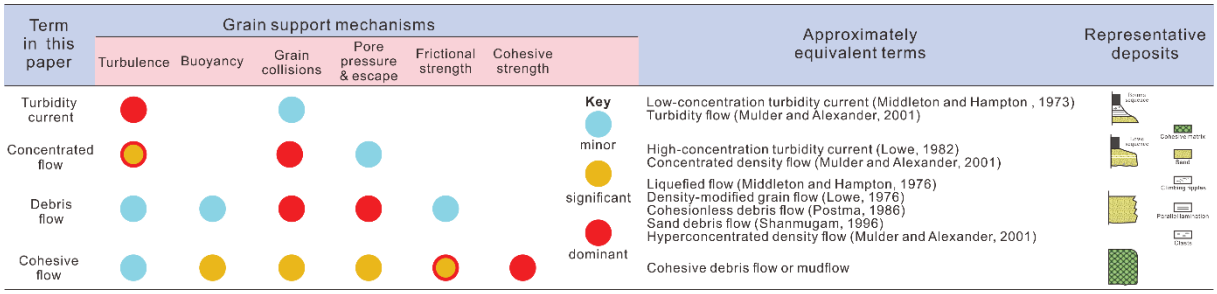

Figure 2. Relative importance of particle-support mechanisms, approximately equivalent terms, and associated sedimentary features of the four types of gravity flow deposits recognized in this paper (modified from Pickering and Hiscott, 2015).

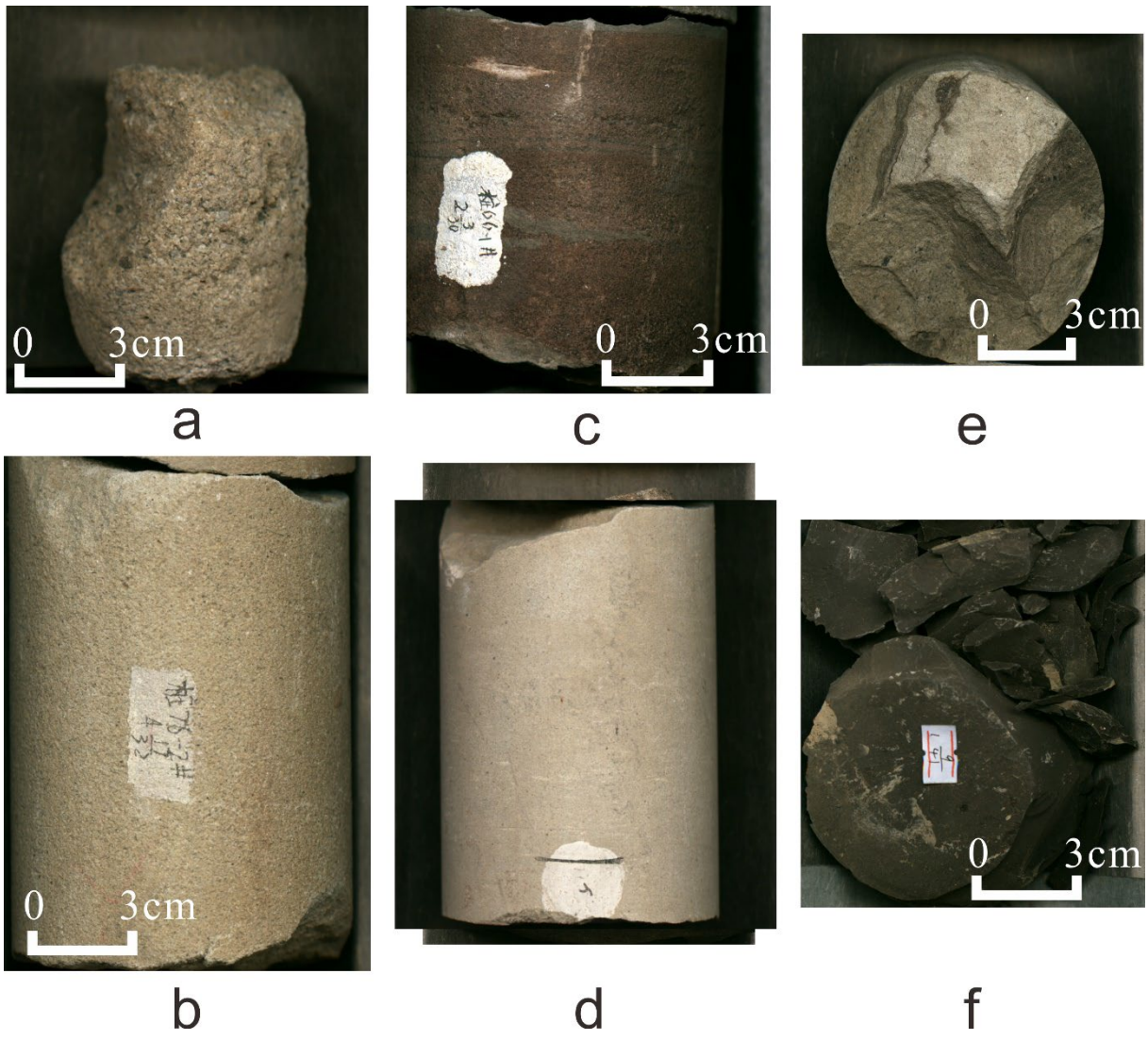

Figure 3. Lithofacies of lacustrine gravity flow deposits in the Gubei Sag. (a) Pebbly sandstone (*fmps*) in well z55 at 3296.38 m; (b) sandstone (*fms*), well z76-2 at 3220.47 m; (c) muddy sandstone (*fcms*), well z66-1 at 3406.76 m; (d) siltstone (*fmss*), well z50 at 3208.79 m; (e) muddy siltstone, well z62 at 3401.49 m; and (f) mudstone, well z76-2 at 3198.8 m.

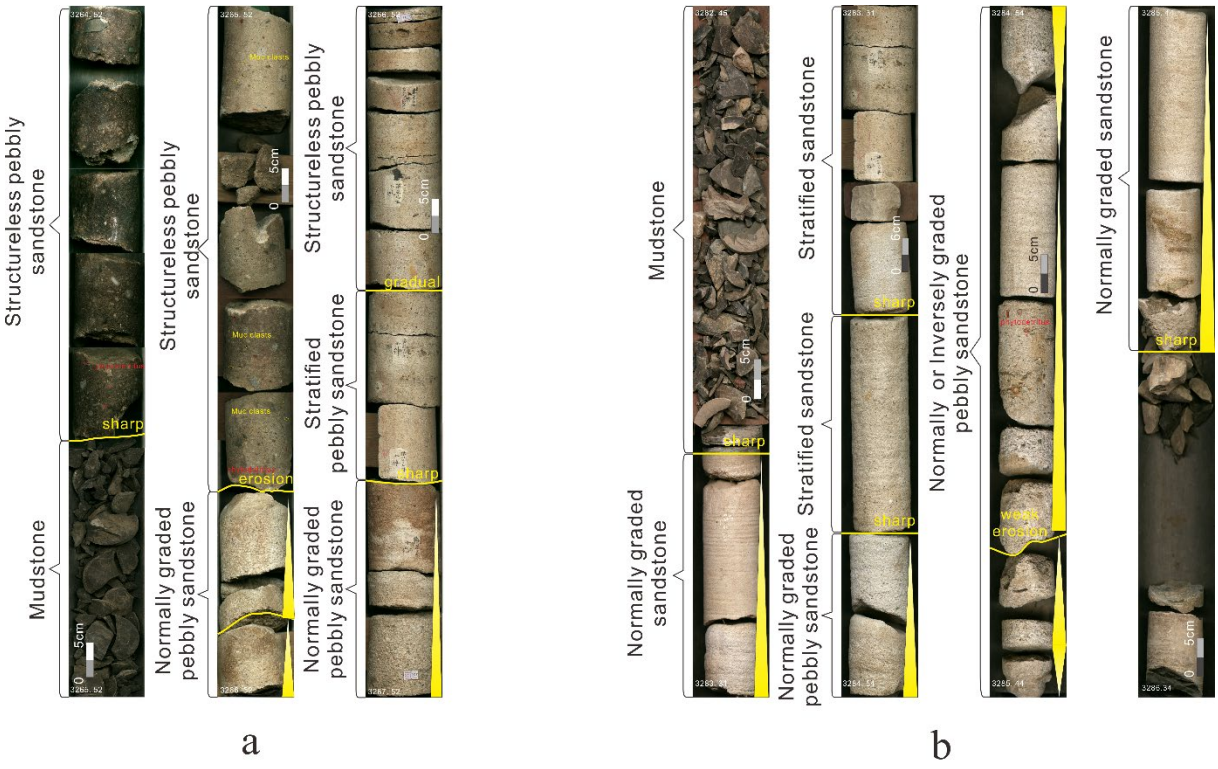

Figure 4. Different sediment beds of pebbly sandstones caused by lacustrine gravity flows in Gubei Sag. (a) Sedimentary characteristics of LA 1 and underlying LA 6 in well z76-2 and (b) sedimentary characteristics of LA 2 and underlying/overlying graded sandstones in well z74-s1.

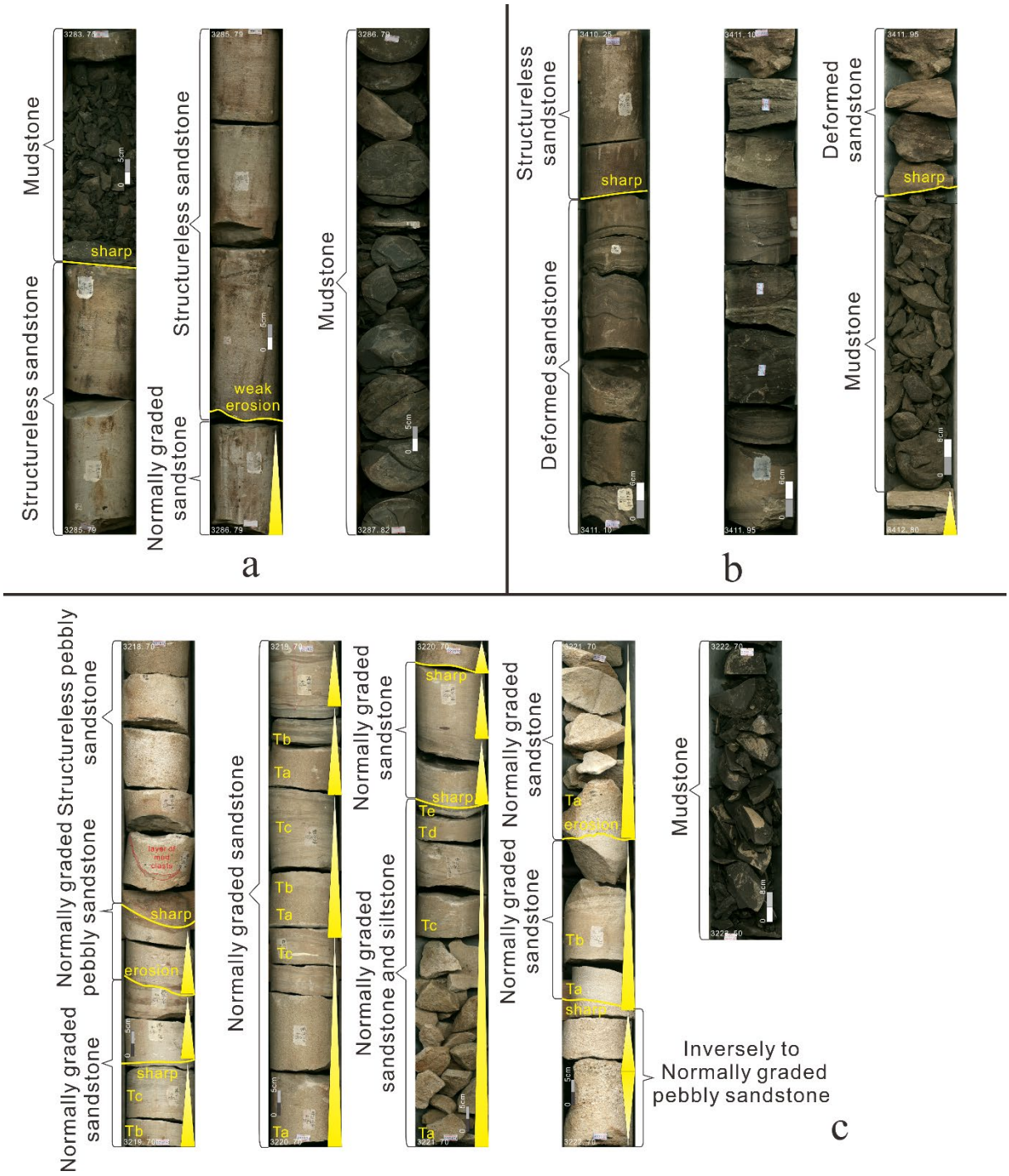

Figure 5. Different sediment beds of sandstones and siltstones caused by lacustrine gravity flows in the Gubei sag. (a) Sedimentary characteristics of LA 3 in well z62; (b) sedimentary characteristics of LA 4 in well z66-1; and (c) the sedimentary characteristics of LA 5 and LA 6 in well z55.

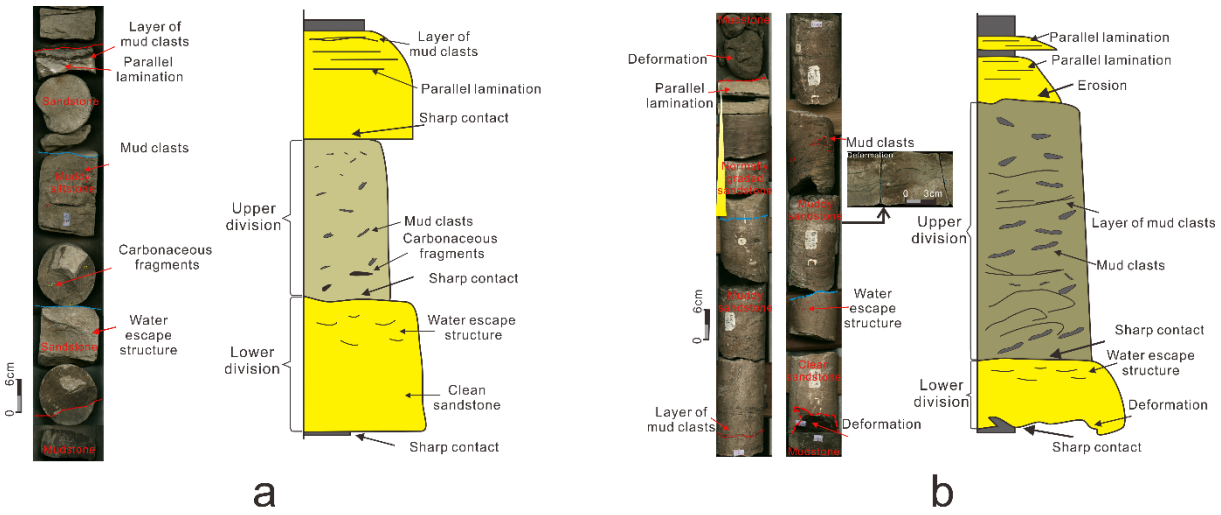

35

36 **Figure 6.** Sedimentary characteristics of various hybrid event beds (HEBs). (a) sedimentary characteristics

37 of LA 7 produced by floating up of low-density debris in well z62; and (b) sedimentary characteristics of LA

38 8 formed by slumping in well z66-1.

39

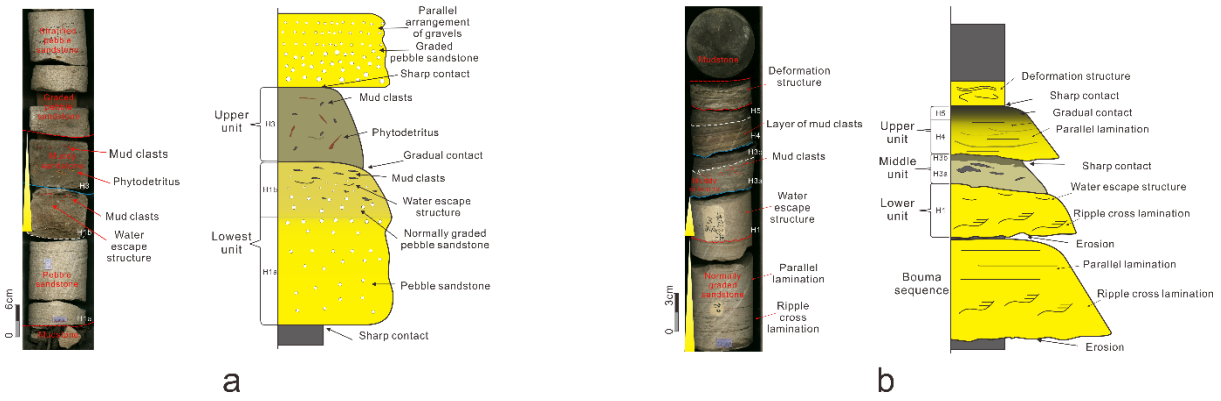

40

41 **Figure 7.** Sedimentary characteristics of different hybrid event beds (HEBs). (a) Sedimentary characteristics

42 of LA 9 caused by particle rearrangement of debris flow in well z62 and (b) sedimentary characteristics of

43 LA 10 derived from the erosion of turbidity currents in well z602.

44

45

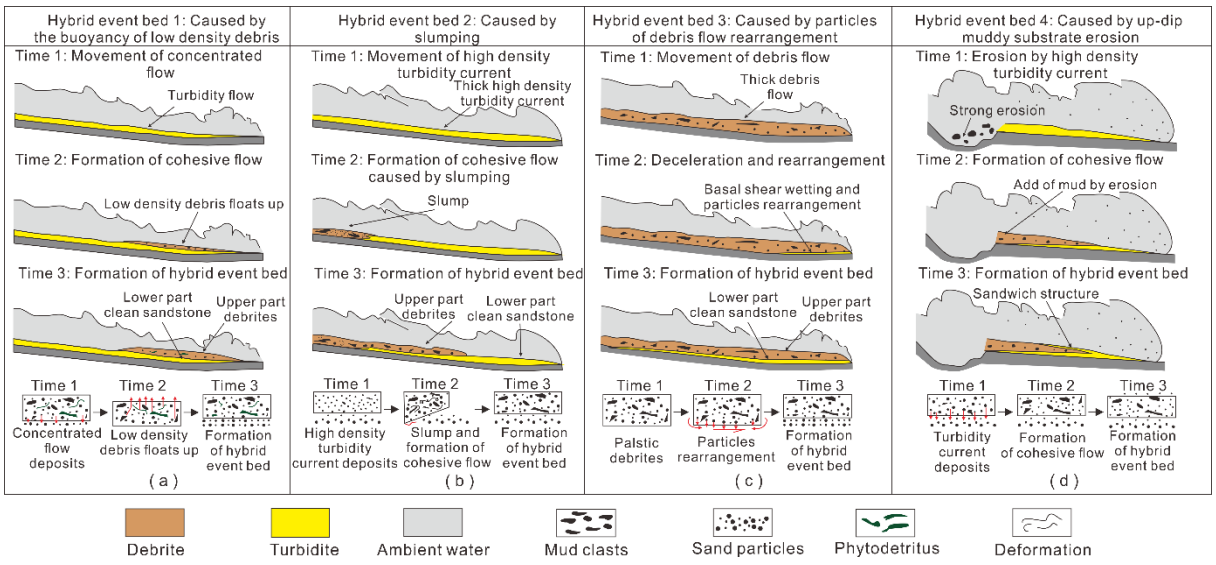

Figure 8. Summary of the origins of hybrid event beds (HEBs) in the Gubei sag (modified from Haughton *et al.,* 2010; Talling *et al.,*2004), displaying the distinct stages and processes of formation of the (a) LA 7; (b) LA 8; (c) LA 9; (d) LA 10.

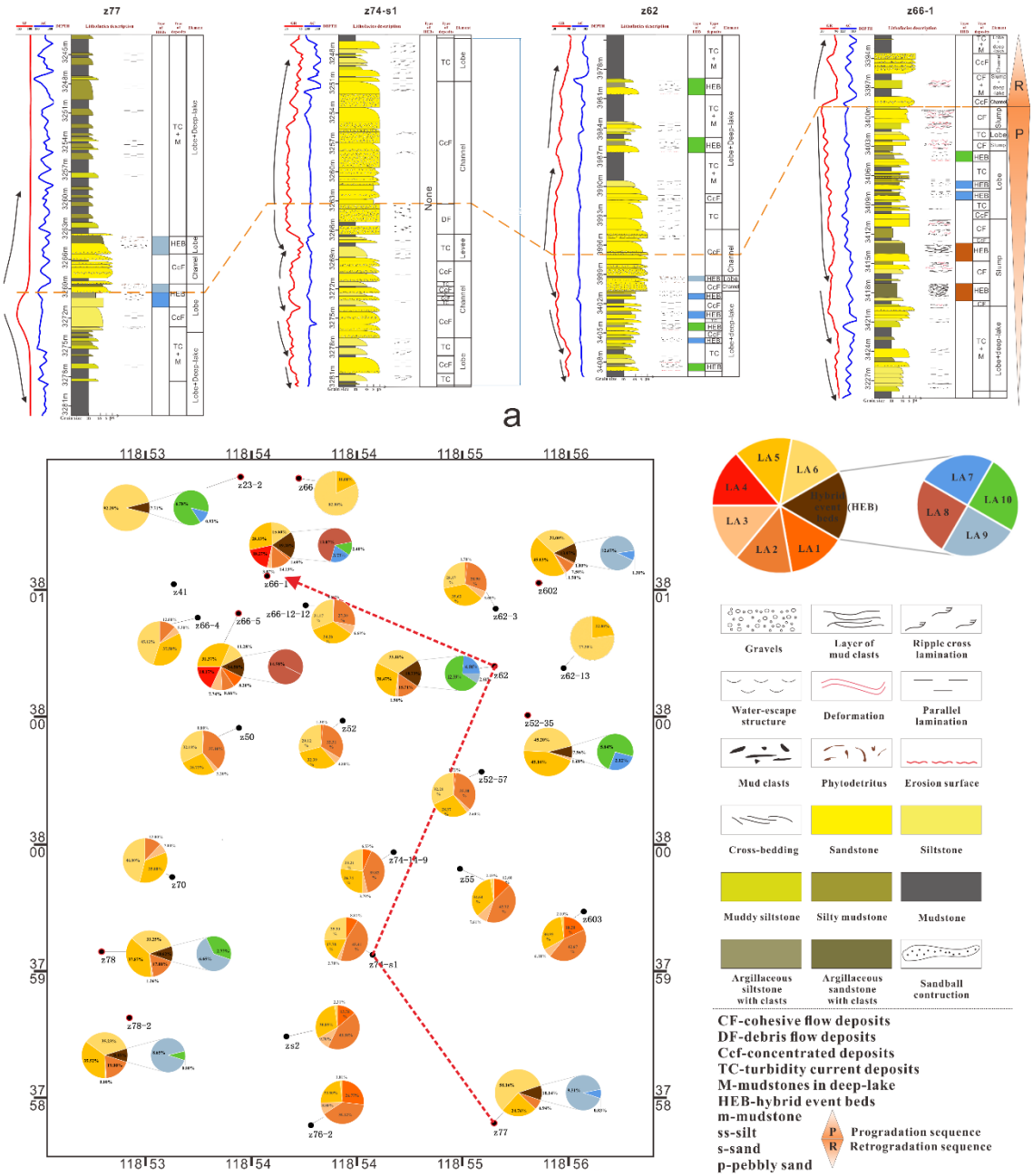

Figure 9. Distribution of distinct types of sedimentary beds. (a) Examples of vertical succession (stacking) of beds; and (b) lateral distribution of beds.

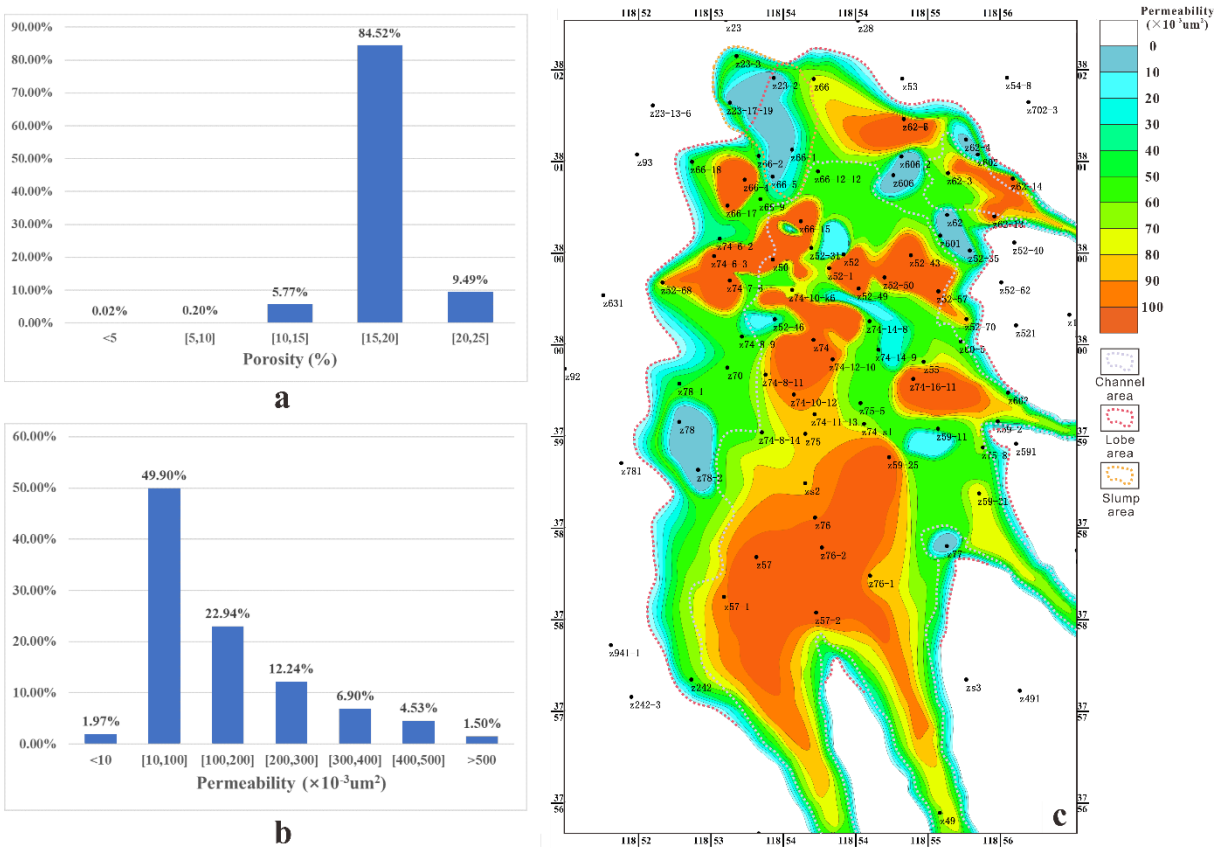

Figure 10. Petrophysical characteristics of lacustrine gravity flow deposits constituting the reservoir in the third member of Shahejie Formation (Es_3) in the Gubei Sag. (a) Porosity histogram; (b) permeability histogram; and (c) permeability lateral distribution.

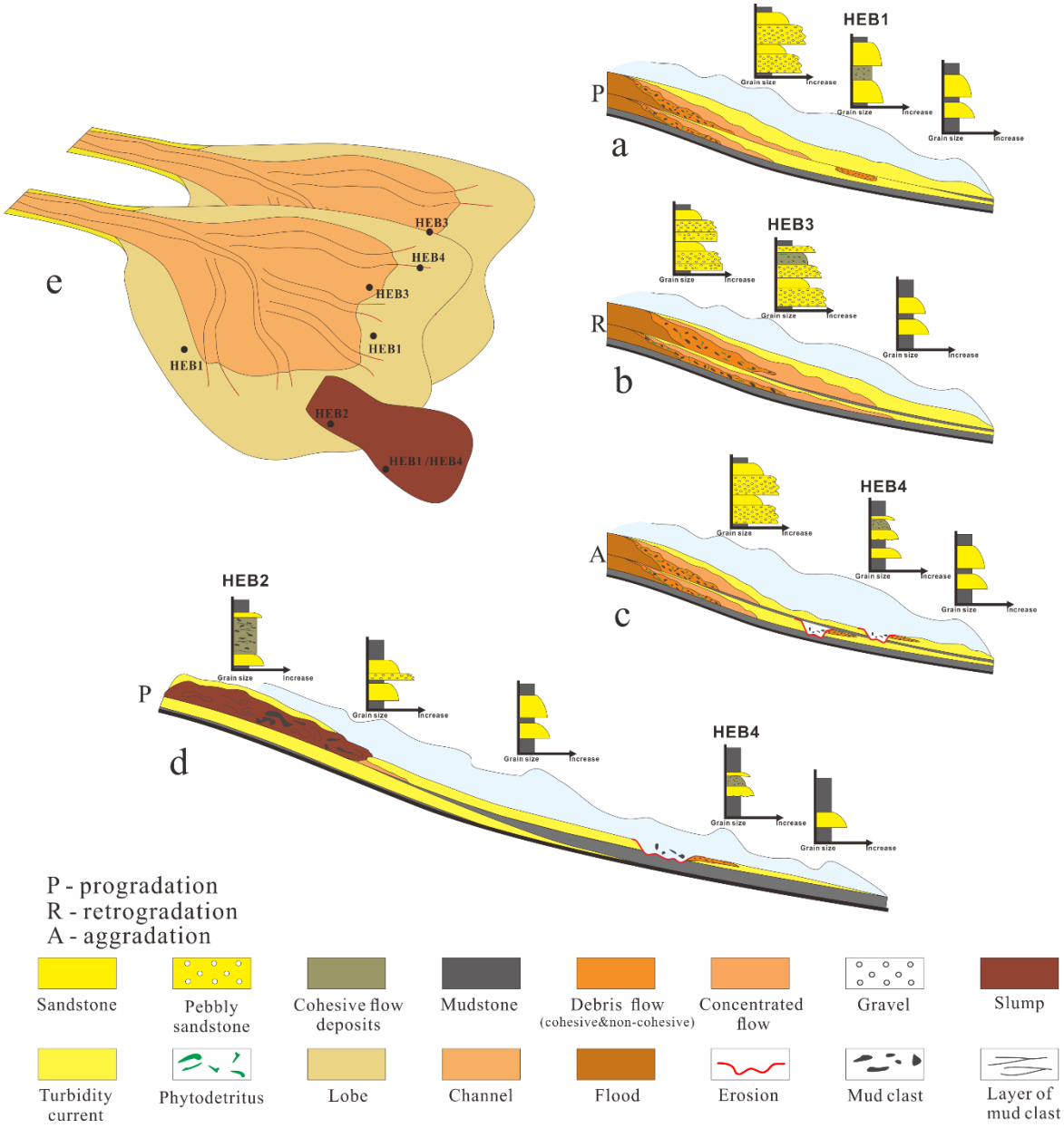

Figure 11. Facies tracts of lacustrine gravity flow deposits resulting from diverse processes: (a) LA 7 (HEB1) produced by floating of low-density debris within turbidity currents; (b) LA 9 (HEB3) derived from the arrangement of particles in debris flows; (c) LA 10 (HEB4) formed by erosion of muddy substrate by turbidity currents; (d) LA 8 (HEB2) derived from slumping processes; and (e) overall distribution of lacustrine gravity flow deposits in the Gubei Sag.

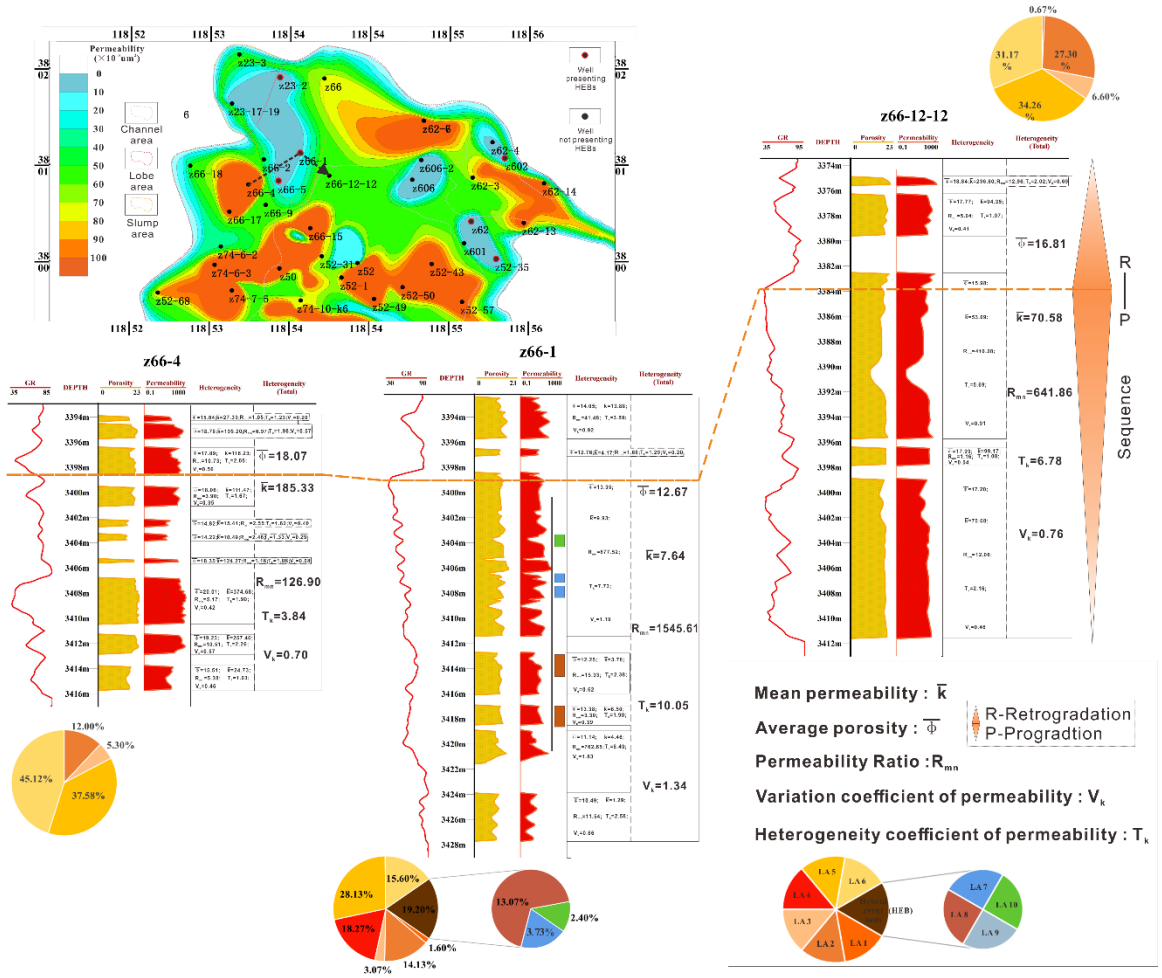

68

69 **Figure 12.** The property and heterogeneity of the reservoir with HEBs in well z66-1 and of the reservoir

70 without HEBs in wells z66-12-12 and z66-4. The much lower porosity and permeability and higher

71 heterogeneity of reservoir in well z66-1 than in wells z66-12-12 and z66-4.